1996-11

How well does a 1/4° global circulation model simulate large-scale oceanic observations?

Stammer, Detlef

Journal of Geophysical Research, Vol. 101, No. C10, pp. 25,779-25,811, November 15, 1996.
http://hdl.handle.net/10945/43802

JOURNAL OF GEOPHYSICAL RESEARCH, VOL. 101, NO. C10, PAGES 25,779–25,811, NOVEMBER 15, 1996

How well does a 1/4° global circulation model simulate large-scale oceanic observations?

Detlef Stammer
Department of Earth, Atmospheric, and Planetary Sciences, Massachusetts Institute of Technology, Cambridge

Robin Tokmakian and Albert Semtner
Department of Oceanography, Naval Postgraduate School, Monterey, California

Carl Wunsch
Department of Earth, Atmospheric, and Planetary Sciences, Massachusetts Institute of Technology, Cambridge

Abstract. Numerical high-resolution ocean general circulation models have experienced a revolutionary development during the last decade. Today they are run globally in realistic configuration with realistic surface boundary forcing. To fully use the results of those models in understanding various aspects of the ocean general circulation and to combine ocean observations with models (state estimation) in a manner consistent with the data and model dynamics, stringent model-data comparisons are a necessary first step. In this paper a quantitative model-data comparison is carried out for the global Parallel Ocean Climate Model (POCM), known also as the Semtner and Chervin model, with nominal lateral resolution of 1/4°. The focus is on various aspects of the simulated large-scale circulation and their relation to the TOPEX/POSEIDON sea surface height (SSH) observations and World Ocean Circulation Experiment (WOCE) hydrography. Comparisons are made for (1) the global mean sea surface circulation and absolute slopes, (2) rms SSH variability and eddy kinetic energy, (3) the simulation of the observed seasonal cycle in SSH, (4) two-dimensional frequency-wavenumber spectra of the large-scale fluctuations, as well as (5) the hydrography for WOCE sections. Recent improvements in external surface forcing fields including daily wind-stress fields and sea surface heat fluxes lead to a significant improvement in the overall agreement of the simulated and observed large-scale mean circulation and its variability. However, simulated amplitudes of variability remain low by about a factor of 2 to 4 over a broad spectral range, including the long wavelengths and periods. Both the causes and consequences of this low variability remain obscure.

1. Introduction

Oceanic general circulation models (OGCMs) have come to play a prominent role in understanding the ocean circulation and its role in climate forecasting. But model results can be unrealistic for many reasons, including incorrect initial conditions, boundary forcing (surface and lateral), inadequate resolution, and missing physics. To make full use of present state-of-the-art OGCMs, it is therefore important that there be thorough testing and widespread understanding of their skill. It is among the goals of World Ocean Circulation Experiment (WOCE) to improve our present OGCMs through appropriate model-data comparisons. Such studies aim to understand the shortcomings of internal model physics, as well as external atmospheric forcing fields, and ultimately will lead to models more suitable for climate prediction than can be achieved presently.

The clearest and most complete understanding of the ocean circulation and its consequences on present climate and climate change will ultimately be obtained through appropriate combinations of dynamical models and direct observations. Procedures for making those combinations fall under the general heading of "estimation theory," or, more narrowly, of "assimilation." Most such combinations represent a weighted average of the observations and model predictions, with the weighting coefficients representing the inferred uncertainties of both data and model. But to obtain meaningful results, the underlying model and observations must be

Paper number 96JC01754.
0148-0227/96/96JC-01754$09.00

statistically consistent. Therefore detailed comparisons of various aspects of the model with data need to be performed, prior to any estimation or assimilation attempt.

Model skill will vary greatly as a function of geographical position but also as a function of frequency and wavenumber, and ultimately, the full frequency-wavenumber range has to be explored. The purpose of this present paper is more modest: It aims only to quantify the skill on large spatial scales of the particular WOCE Parallel Ocean Climate Model (POCM) [*Semtner and Chervin*, 1992] with a nominal lateral resolution of 1/4°. The focus is on the upper ocean large-scale circulation as observed by the TOPEX/POSEIDON altimetry and the WOCE hydrography, data sets which have only recently become available to oceanographers on the global or at least basin scale. Both the time mean and the low-frequency variability are examined, with particular emphasis on the annual cycle. Studies of model-data differences are usually complicated by the existence of complex data errors with sometimes unknown structures. Therefore comparisons such as those performed here, simultaneously serve also to illuminate errors in the observations. A comparison complementary to ours was performed by J. McClean, A. Semtner, and V. Zlotnicki (Comparisons of mesoscale variability in the Semtner-Chervin quarter-degree and the Los Alamos POP sixth-degree models and TOPEX/POSEIDON data, submitted manuscript, 1996; hereinafter referred to as McClean et al., submitted manuscript, 1996), who studied eddy scale variations in TOPEX/POSEIDON data and high-resolution models.

The paper is organized as follows: in the next section we will summarize the model, the TOPEX/POSEIDON altimeter data, and the WOCE hydrography. The time-mean circulation and its variability will be compared in sections 3 and 4, respectively. Section 5 focuses on the representation of the observed seasonal cycle in the model.

2. Model and Data Description

2.1. The Model

Semtner and Chervin [1992] describe the basic model formulation. Significant differences in the present form include an improvement in the lateral resolution to a Mercator grid size of 0.4° in longitude allowing square grids everywhere between the equator and 75° latitude. A resulting average grid size is 0.25° in latitude. The model bottom topography was created from a bathymetric data set at a resolution of 1/12° by averaging the depth values which fell within a model grid box. A free surface has been incorporated using the formulation of *Killworth et al.* [1991], which treats the sea level pressure (or equivalently the surface elevation) as a prognostic variable.

Two separate model runs exist now in the above global configuration with 1/4° spatial resolution, which are distinct in their surface forcing formulations for wind-stress and heat flux. The first run, POCM_4A, was performed over the period 1986 through 1989 using monthly mean wind-stress fields (provided by A. Craig at National Center for Atmospheric Research (NCAR)) and simple *Haney* [1971] restoring of T and S fields in the uppermost of the 20 levels toward a monthly mean *Levitus* [1982] T_{Lev} and S_{Lev} climatology with restoring timescale $\gamma = 30$ days, to simulate surface heat and salt fluxes. For this purpose, the *Levitus* [1982] monthly temperature and salinity fields were interpolated on to the model grid with 3 day time step, using a bicubic spline fit first in space and then time.

The second calculation, POCM_4B, was run for the period 1987 through 1994 forced by daily wind-stress fields derived by the European Center for Medium-Range Weather Forecasts (ECMWF) (again provided by A. Craig) as well as monthly mean sea surface heat fluxes produced by *Barnier et al.* [1995] from ECMWF analyses with zero global, annual mean, in addition to a *Haney* [1971] T, S surface restoring terms. Flux fields were incorporated as

$$\frac{dT}{dt} = \frac{Q(t)}{\rho_0 c_p h} + \gamma^{-1}(T_{\mathrm{Lev}} - T), \qquad (1)$$

where $Q(t)$ denotes the monthly surface heat flux climatology, c_p the specific heat of seawater, and h the depth of the top model layer. For the surface restoring of T and S, the recent, and improved, *Levitus et al.* [1994] monthly surface T_{Lev} and S_{Lev} fields are used, again with a $\gamma = 30$ days timescale.

To mimic the exchange of water mass properties with those areas not included in the model domain, both model runs use a subsurface restoring of T and S fields toward similar *Levitus* [1982] fields over the top 2000-m depth range with lateral extent between 58° and 65°N and between 68° and 75°S, along the northern and southern artificial boundaries, respectively (equivalent to 37 and 57 grid points, laterally). A similar restoring zone is located near Gibraltar. The lateral restoring timescale was $\gamma = 120$ days.

The monthly wind-stress fields used for POCM_4A were created from fields of ECMWF 1000-mbar twice daily winds, converted to wind-stress [*Trenberth et al.*, 1989]. Resulting monthly mean fields from the period 1986 through 1989 were interpolated on to the model grid with a 3 day time step, using a bicubic spline fit in space and time, respectively.

It was shown by *Mestas-Nuñez et al.* [1994] that the *Trenberth et al.* [1989] wind-stress amplitudes are globally high by about 40% because stress fields were derived from 1000-mbar levels, rather than sea level. This deficiency was corrected in the wind-stress forcing for the POCM_4B run, which was derived from 10-m level, twice daily ECMWF wind fields for the period 1987 through 1994. Daily wind-stress fields were averaged over 3 days for use in the model.

To begin, a previous 1/2° version of the model was spun up for 33 years starting from the *Levitus* [1982] T and S distribution. Initial conditions for POCM_4A were obtained from an instantaneous 1/2° model state at the end of the 33 years, interpolated to the 1/4

grid, and equilibrated with 1985 ECMWF winds. It was then integrated over the period 1986-1989. Finally, POCM_4B was started from a model state at the end of POCM_4A and run over the period 1987 through 1994. The problem of model equilibration during the 40 years of model spin-up prior to the period 1993/1994 analyzed in this study will be addressed in a separate section below.

The model time step for the first run was 10 min. As a result of several changes suggested by R. Smith, B. Malone, and J. Dukowicz from Los Alamos National Laboratory (personal communication, 1994), it was possible to increase the baroclinic time step of POCM_4B to 30 min., achieved by a pressure averaging scheme [*Brown and Campana*, 1978]. In the same run, the barotropic time step was 30 s. Vertical viscosity is handled through the *Pacanowski and Philander* [1981] formulation. Note that the equation of state differs in the two model runs, with the new model using the *Bryan and Cox* [1972] equation of state, which improves the accuracy at low temperatures.

Diffusion is handled using biharmonic closure for both momentum and tracers. The momentum coefficient is 1.1×10^{20} cm^4/s, and the tracer coefficient is 5×10^{19} cm^4/s, both scaled by $\cos^{2.25}(\phi)$, with ϕ being geographical latitude, to reduce mixing at high latitudes. This is an important aspect for a later interpretation of model results.

Data fields for horizontal and vertical velocity, temperature, salinity, surface height, and barotropic speed are stored every 3 days. Statistics, such as eddy kinetic energy, means, and standard deviations, are computed from the different fields for monthly, annual, and total ensemble statistical maps after the model runs were completed. (Details of both runs, including animations, can be viewed via the World Wide Web (WWW) page, http://vislab-www.nps.navy.mil/~rtt.)

A comparison of results from POCM_4A and POCM_4B revealed that the latter run, driven by daily wind-stress fields and improved surface heat fluxes, leads to a superior agreement with TOPEX/POSEIDON observations. Comparisons presented below are therefore based primarily on POCM_4B, but results from both model runs are displayed in Figure 6 and Table 2 to illustrate the degree of alteration from the prior configuration.

2.2. TOPEX/POSEIDON Altimetry

The French/U.S. joint TOPEX/POSEIDON (T/P) mission was specifically designed to observe the large-scale ocean circulation and its variability. Previous studies (see the T/P special issues of *Journal of Geophysical Research, Oceans*, C12, December 1994 and C12, December 1995) all showed that the accuracy and precision of the instrument are significantly better than project specification and are currently at the 2-cm level. *Fu et al.* [1994] describe the mission characteristics and performance and provide a preliminary error estimate.

T/P data from the 2-year period December 11, 1992, to December 5, 1994, corresponding to repeat cycles 9 through 81, were edited and corrected as described by *Stammer and Wunsch* [1994] and *King et al.* [1994]. Three significant modifications of the standard merged T/P geophysical data records [*Benada*, 1994] should be noted here because they influence the results and the underlying uncertainties. First, to obtain observations of the absolute dynamic sea surface height (SSH), we referenced the T/P observations to a hybrid Joint Gravity Model-3 (JGM-3) Ohio State University (OSU91a) geoid, where the former is used to spherical harmonic degree 70 and the latter beyond that to degree 360. The JGM-3 geoid model is developed by the T/P project [*Tapley et al.*, 1994] as an improved version of the prelaunch JGM-2 model [*Nerem et al.*, 1994], and the OSU91a model stems from *Rapp et al.* [1991]. Second, the tidal correction provided by the T/P project was replaced by those estimated by the University Texas/Center for Space Research Group *Ma et al.* [1994] from the first 2 years of T/P data in their version 3.0. Lastly, we used JGM-3 model based orbit calculations with significantly reduced radial and geographically correlated orbit errors [*Tapley et al.*, 1996]. The resulting mean field of this 2-year period is shown in Plate 1b after gridding by averaging the along-track data in 2° x 2° geographical areas and after applying a *Shapiro* [1970] low-pass filter to remove spurious stationary small scale structures related to geoid errors [see *Stammer and Wunsch*, 1994].

2.3. WOCE Hydrography

Hydrography will be used in two different ways as a comparison data set. An absolute surface velocity field computed by *Macdonald* [1995] from a global inversion of hydrographic and nutrient data along various hydrographic sections is used to produce absolute elevation estimates along trans-oceanic lines. Five (two in the Atlantic and three in the Pacific) zonal WOCE hydrographic lines will be compared to the model temperatures and salinities. Table 1 lists the details for all hydrographic sections. The model months that have been used for comparison to the hydrographic data are, for P1, June 1988; P3, April 1988; P4, April 1989; A9, March 1991; and A11, February 1992. Note that two of the five lines were measured prior to the model time period. For those two lines, the corresponding month in the earliest year of the POCM_4B run was used for a comparison (see section 3.2). Because in most cases the in situ data are provided with higher horizontal and vertical resolution than present in the model, the in situ data were averaged vertically on to the model depths level and subsequently interpolated horizontally on to the model grid.

3. The Mean Circulation

3.1. TOPEX/POSEIDON

We begin by examining the time mean ocean circulation as it results from POCM_4B (Plate 1a) and as inferred from T/P observations and the JGM-3 geoid (Plate 1b), both fields averaged over the identical pe-

Table 1. Details on the Zonal Hydrographic/Conductivity-Temperature-Depth (CTD) Sections

Basin	Latitude	Ship and Reference	Name	Season	Profiles
Pacific	47°N	RV *T. Thompson*, *Talley et al.* [1991]	P47N/P1	summer 1985	115
	24°N	RV *T. Thompson*, *Roemmich et al* [1991]	P24N/P3	spring 1985	212
	10°N	RV *Moana Wave*, *Wijffels* [1993]	P10N/P4	spring 1989	217
	28°S	*Scorpio Eltanin* 29, *Stommel et al.* [1973]	P28S	summer 1967	99
	43°S	*Scorpio Eltanin* 28, *Stommel et al.* [1973]	P43S	spring 1967	76
Indian	12°S	AODC, *You and Tomczak* [1993]	Mz_N	spring 1965	6
	15°S	AODC *You and Tomczak* [1993]	Mz_S	spring 1965	4
	18°S	*Atlantis* II 93, *Warren* [1981]	I18S	summer 1976	57
	32°S	RRS *Darwin*, *Toole and Warren* [1993]	I32S	winter 1987	106
Atlantic	48°N	*Hudson* 82, *Hendry* [1989]	A48N	spring 1982	78
	36°N	*Atlantis* II 109 leg 1, *Roemmich and Wunsch* [1985]	A36N	summer 1981	101
	24°N	*Atlantis* II 109 leg 3, *Roemmich and Wunsch* [1985]	A24N	summer 1981	89
	11°N	*Oceanus* 338,*Friedrichs and Hall* [1993]	A11N	spring 1989	85
	11°S	*Oceanus* 133 leg 5, M. McCartney (personal communication, 1994)	A11S	spring 1983	82
	23°S	*Oceanus* 133 leg 3, M. McCartney (personal communication, 1994)	A23S	winter 1983	99
	17°S	SAVE *Knorr* leg 3, *Scripps Institution of Oceanography* [1992a]	A27S	winter 1988	33
	40°S	SAVE *Melville* leg 4c, *Scripps Institution of Oceanography* [1992b]	A27S	winter 1989	21
	65°S	*Meteor* 11/5, *Roether et al.* [1990]	A57S	winter 1990	78
	19°S	*Meteor* 15/3, *Siedler and Zenk* [1992]	A9	winter 1991	112
	45°S	*Discovery* 199, *Saunders et al.* [1993]	A11 Drake 0E2Afr	winter 1992	28
		RV *Knorr*, *AJAX Expedition* [1985]	0E	winter 1983	137
		RV *Conrad* 17, *Jacobs and Georgi* [1977]	30E	fall 1974	53
		USNS *Eltanin* 41, *Nierenberg et al.* [1970]	132E	winter 1969	19

AODC is the Australian Oceanography Data Centre. SAVE is the South Atlantic Ventilation Experiment.

riod in 1993/1994 (repeat cycles 9 through 81). Here a major issue is data, rather than model, error.

Elements of the general circulation present in the T/P observations (based on the older JGM-2 geoid) and uncertainties are discussed in some detail by *Stammer and Wunsch* [1994]. We restrict ourselves here to the statement that the global circulation is evident in the T/P estimates but that major discrepancies are present in the altimetric absolute mean field owing to geoid errors. A comparison of Plate 1b with Plate 1a of *Stammer and Wunsch* [1994] indicates the degree of improvement obtained recently in the estimate of a mean SSH through geoid model refinement. This improvement is most readily apparent in the tropical Pacific, where an artificially high mean SSH resulted from errors in the JGM-2 geoid. But significant changes can likewise be found in all other ocean basins (R.H. Rapp, Comparison and assessment of the geoid undulations implied by the OSU91A, JGM-2, and JGM-3 potential coefficient model, unpublished manuscript, 1995).

The difference between the T/P results and the mean model field is shown in Plate 1c. Apart from the Southern Ocean where the largest differences are visible, discrepancies are found primarily on relatively small scales. There are strong inconsistencies visible close to continental boundaries and major oceanic trench systems, e.g., the Philippine and Puerto Rico trenches which are all regions of large known errors in the geoid estimates (see, for example, Figure 7 of *Rapp et al.* [1991]). The primary source of short-scale model-T/P discrepancy is therefore the geoid error. But model errors are present, as well. Prominent examples are the pronounced ridge-trough system in the tropical Pacific, which is related to a relatively strong North Equatorial Current in the model, and the pronounced high in the North Atlantic, where the model displaced the path of the North Atlantic Current by about 10° zonally (compare Figure 1f).

Despite the apparent geoid-related problems, the model-data differences have been visibly reduced through the improved wind-stress and heat flux forcing. This improvement is especially marked in the Southern Ocean, where the more accurate equation of state may also contribute (compare Plate 2b of *Stammer and Wunsch* [1994]). The global root-mean-square difference in Plate 1c, weighted by area, is about 16 cm, as opposed to 25 cm obtained from POCM_4A relative to the same T/P mean field.

To summarize, the geoid estimates remain inadequate to use altimetric data for improving directly the existing knowledge of the large-scale circulation.

3.2. Comparison With Hydrography

For a more quantitative model test, Figure 1 shows a comparison of the absolute SSH from both T/P and model mean fields with an estimate of the absolute sea level along various WOCE and pre-WOCE lines in the Pacific, Atlantic, and Indian Oceans (see Table 1) as it results from a global inversion of hydrographic and nutrient data [*Macdonald*, 1995; *Macdonald and Wunsch*, 1996]. A mean value was subtracted from each

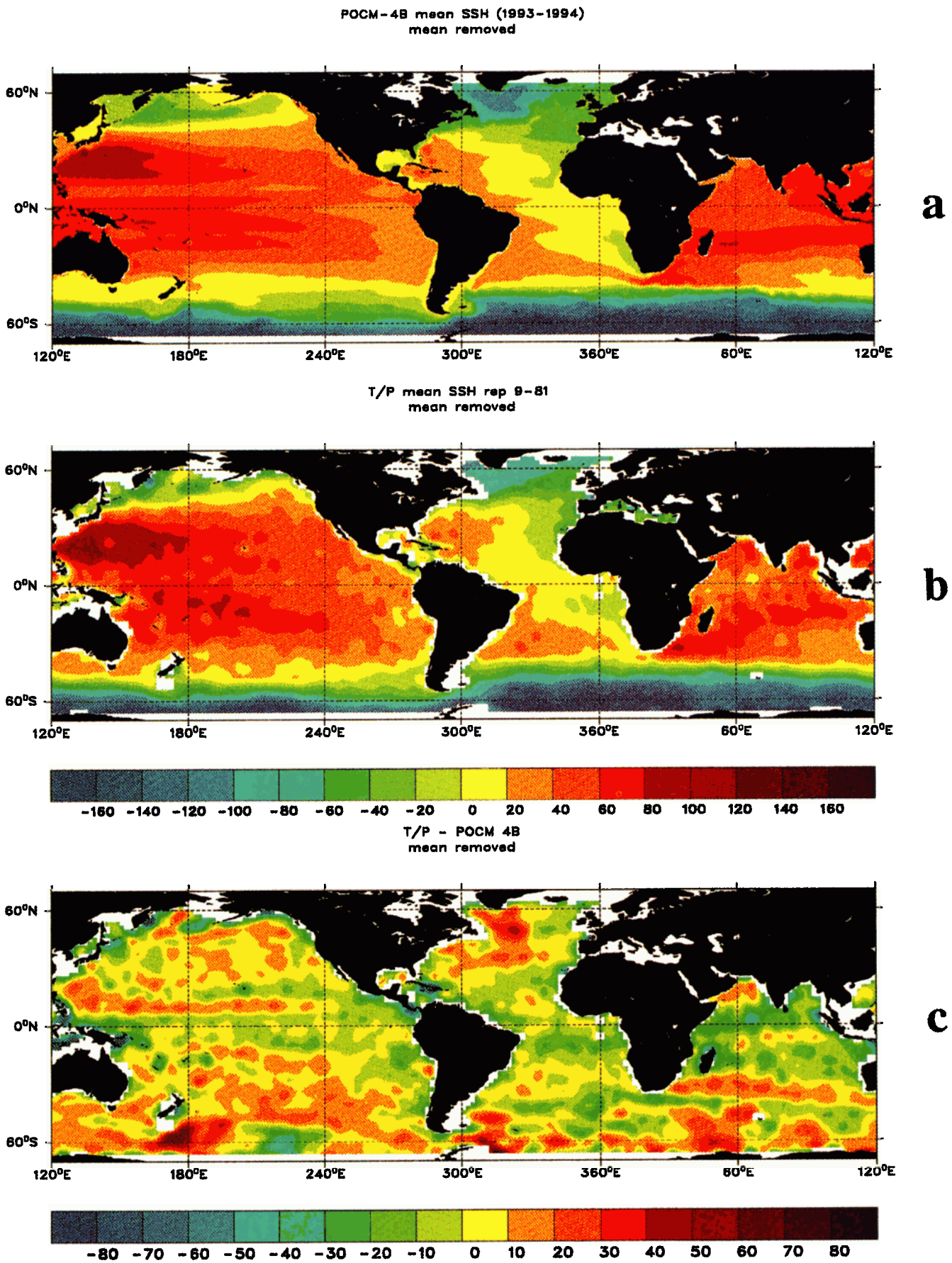

Plate 1. (a) POCM_4B mean sea surface height field from 2-year period 1993/1994. (b) TOPEX/POSEIDON (T/P) mean sea surface height relative to the JGM-3/OSU91a geoid model and averaged over the 2-year period repeat 9 through 81. (c) Difference between the T/P mean field and the model mean. All three fields are on a 2° x 2°grid. Contour intervals are 20 cm in the top two panels and 10 cm in the bottom panel.

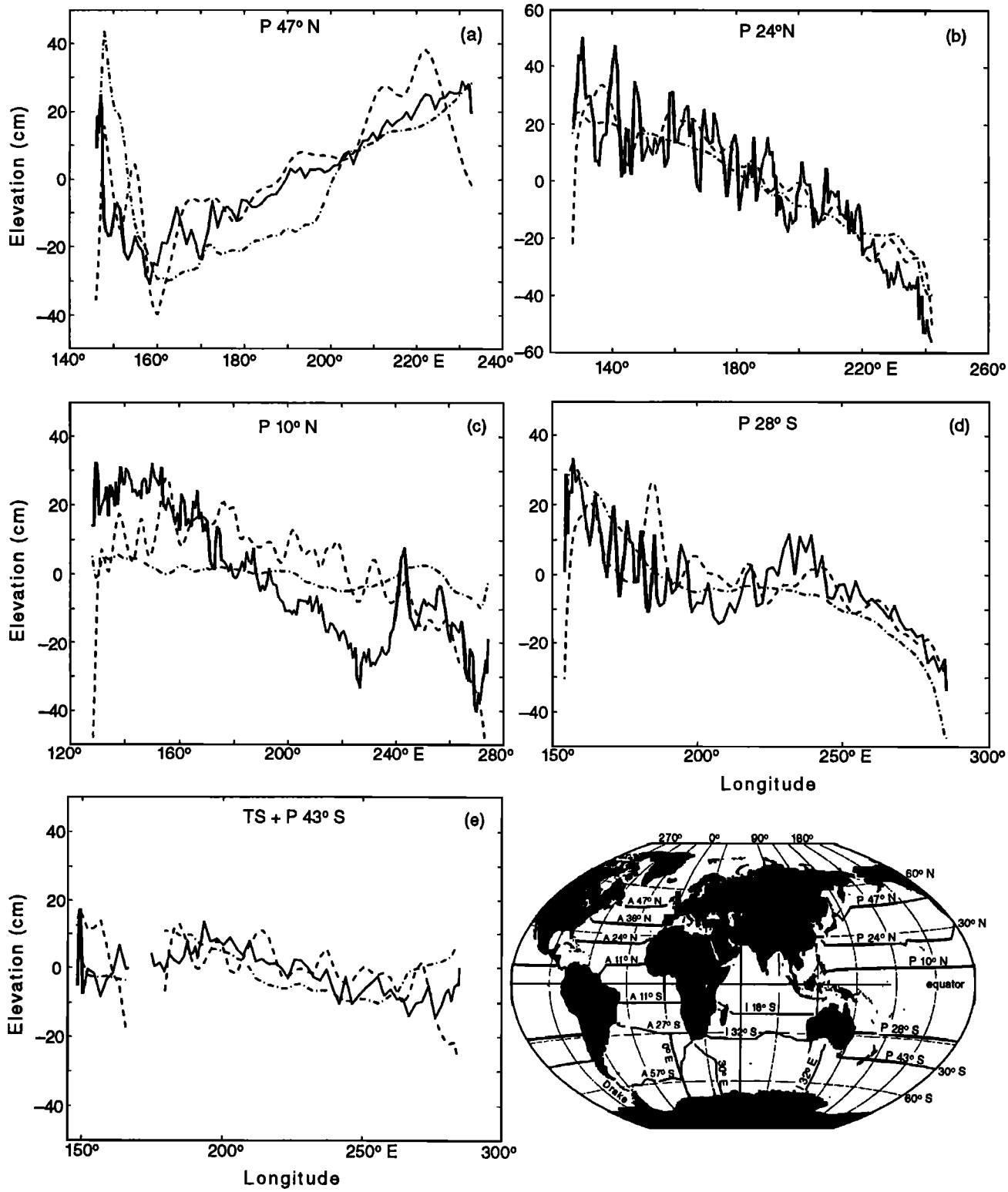

Figure 1. Mean sea surface height from T/P (dashed lines) and POCM_4B (dashed-dotted lines) along various World Ocean Circulation Experiment (WOCE) sections indicated in the panels, together with an estimate of absolute sea surface height from an inversion of hydrographic and nutrient data (solid lines; from *Macdonald* [1995]).

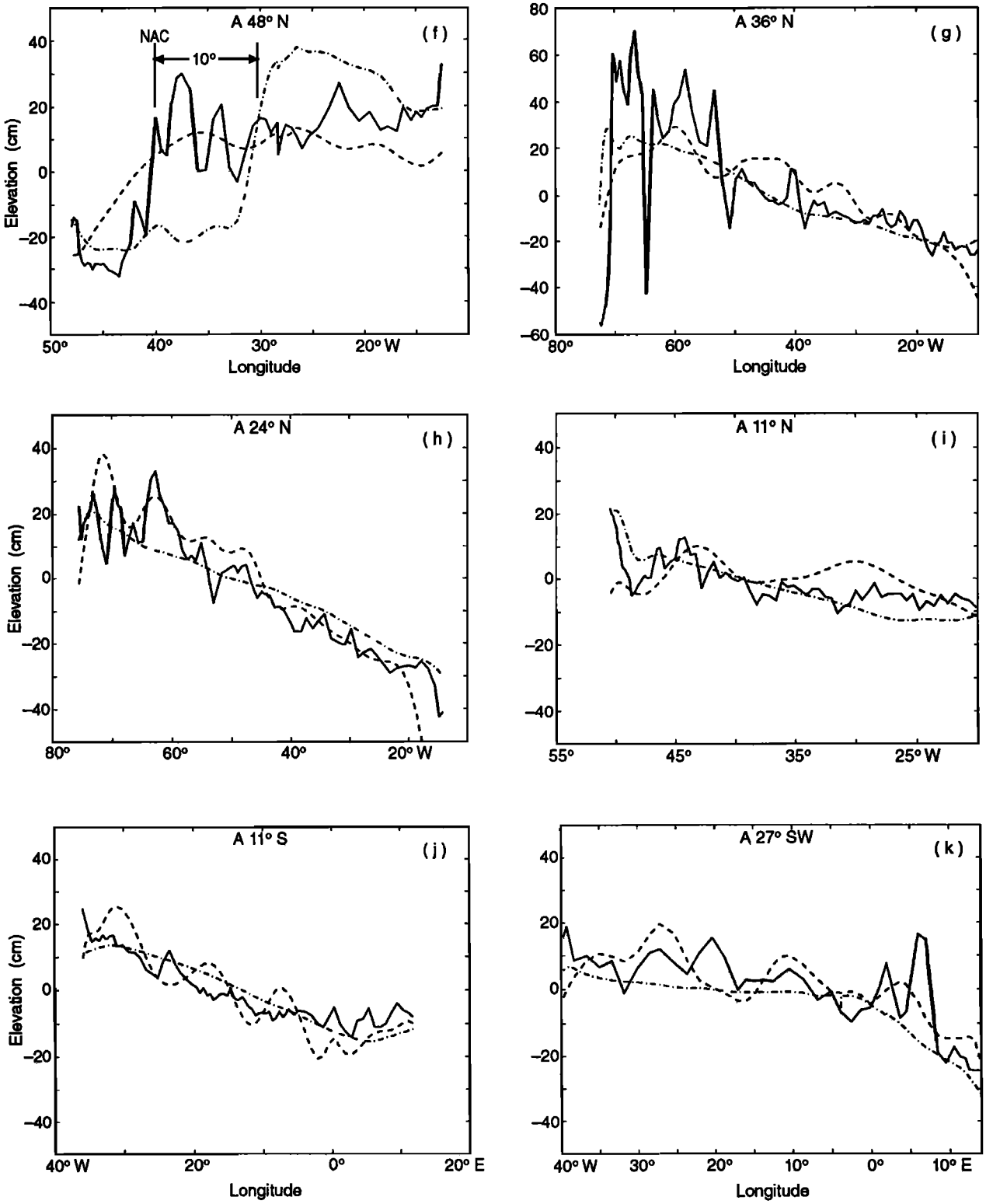

Figure 1. (continued)

curve to account for a missing absolute constant in the hydrographic estimates. Table 2 lists the root-mean-square (rms) differences and cross correlations between all three individual fields. To indicate differences between the model mean fields from the two runs, the statistics of POCM_4A (averaged over 1986 through 1989) relative to the hydrography are included in Table 2.

The formal errors of *Macdonald*'s [1995] results on scales larger than the mesoscale are $O(1$ cm). (This small error can be understood by noting that a 1 cm surface elevation change in a water depth of 5000 m leads

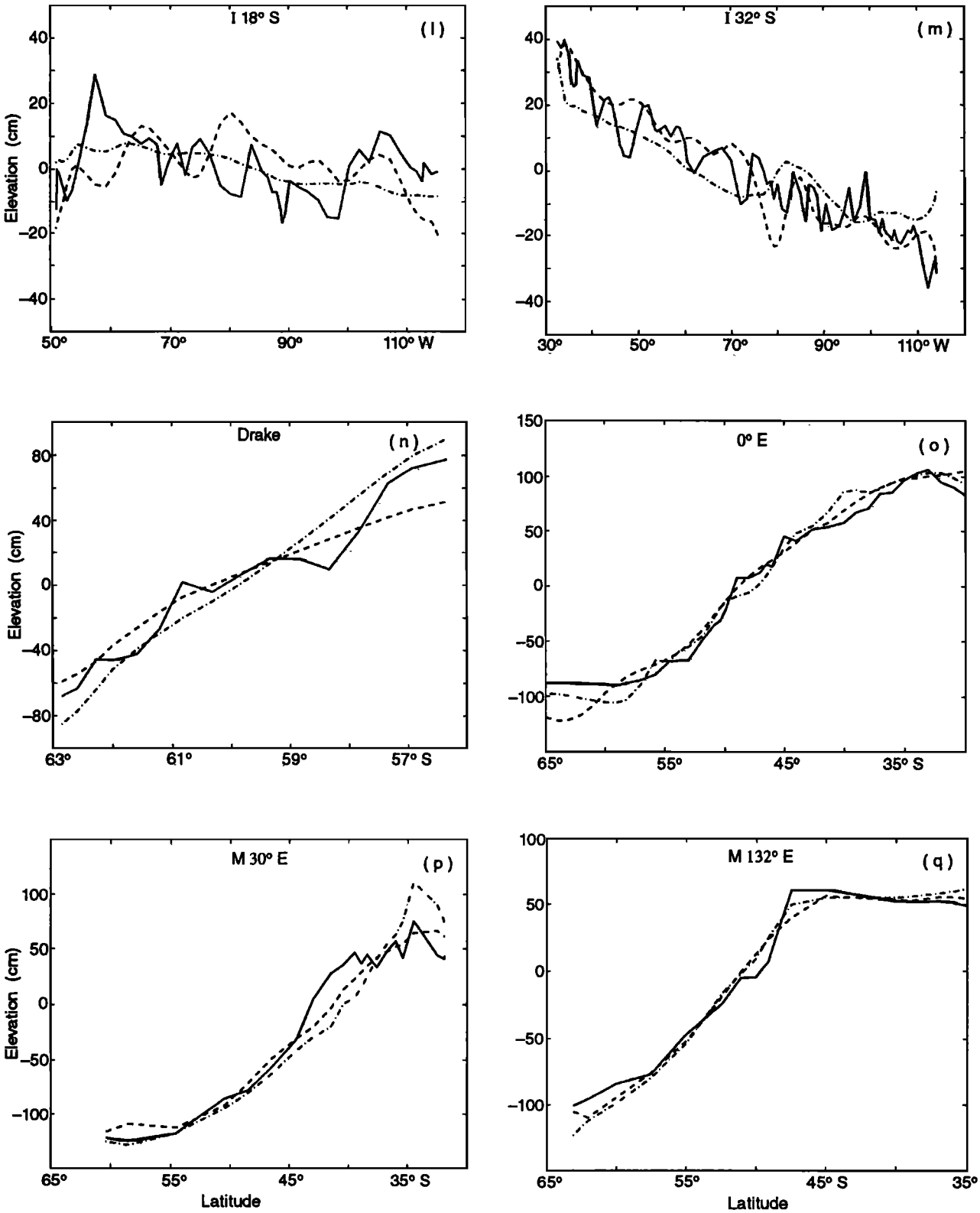

Figure 1. (continued)

to a basin integrated mass flux of $O(7$ Sv) and Macdonald's large-scale mass flux errors are formally estimated as about 2 Sv (Sv $= 10^6$ m^3/s).) But systematic errors in the Ekman flux arising from problems with the wind fields, which are not accounted for in the formal error, can significantly raise the actual uncertainty above the formal value. Errors owing to mesoscale variability in the hydrography will exceed 10 cm. T/P data, on the other hand, are also increasingly noisy at smaller scales. According to *Nerem et al.* [1994], geoid errors exceed

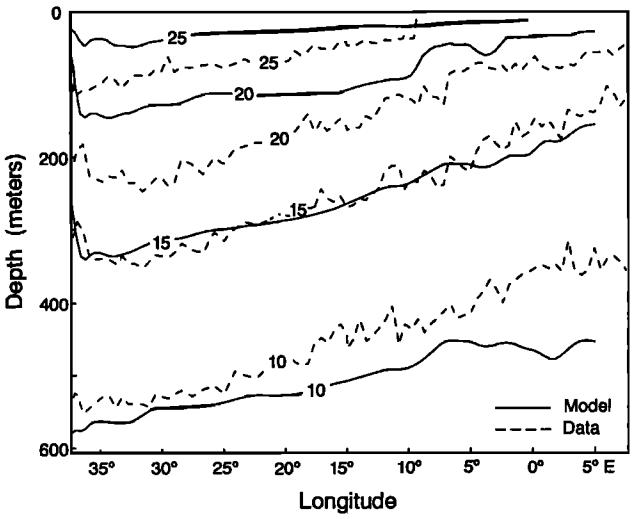

Figure 2. Temperature section from the POCM_4B model along the Atlantic WOCE line A9, 19°S (solid contours) shown together with the observations (dashed contours).

the ocean circulation signal at wavelengths below 2000 km, approximately. Although the space/time average of the hydrography is not completely consistent with the two-dimensional averaging implicit in the altimetry (see A. Ganachaud, C. Wunsch, M.-C. Kim, and B. Tapley, Combination of TOPEX/POSEIDON data with a hydrographic inversion for determination of the oceanic general circulation, submitted to *Geophysical Journal International*, 1996), we see that all three estimates, obtained from completely different sources of information, generally agree with each other to within about 10 cm over most of the oceans. This indicates a remarkable achievement in observing and modeling the ocean circulation and the marine geoid over the past decade. The direct hydrographic inversions remain, however, as the most accurate large-scale estimates that we have.

Some details are noteworthy and help to identify uncertainties in both T/P and model estimates. A striking agreement between the model and the hydrography is obvious in the low-latitude Atlantic, where rms differences are less then 7 cm and to a large extent are attributable to the eddy component in the hydrographic estimates. A remarkable (and perhaps coincidental) agreement between all three estimates is also apparent across various locations of the Antarctic Circumpolar Current (ACC). This result is noteworthy for several reasons. Models are known for overestimating the ACC transport and related sea surface slope by up to a factor of 2. The high-latitude southern hemisphere is also a region of poor satellite tracking coverage and thus of expected enhanced geoid error.

Although model improvements from POCM_4A to POCM_4B are generally associated with a weakened strength of the circulation, a somewhat too vigorous model circulation is still present, most clearly in the section along 47°N (Figure 1a) and 10°N (Figure 1c) in

Table 2. Comparison of Estimates of the Absolute Mean Sea Surface Height Along Zonal Sections

	Correlation Coefficient				RMS				
Section	T/P,Hyd	T/P,4B	4B,Hyd	4A,Hyd	T/P,Hyd	T/P,4B	4B,Hyd	4A,Hyd	Points
a11n	0.13	0.04	0.84	0.82	8.5	11.2	5.7	4.8	70
a11s	0.87	0.91	0.88	0.95	6.6	5.6	4.7	3.6	73
a23s	0.90	0.95	0.95	0.95	5.4	3.8	4.7	4.1	73
a24n	0.87	0.90	0.94	0.95	13.7	14.0	7.4	5.9	85
a27s	0.69	0.81	0.79		8.9	6.0	7.6		46
a36n	0.67	0.76	0.55	0.56	21.9	12.2	24.5	24.8	89
a48n	0.81	0.59	0.67		13.0	20.0	18.7		68
a57s_e	0.60	-0.01	0.52	0.53	8.0	22.4	17.5	14.9	23
a57s_w	0.28	0.30	0.17	0.19	16.0	15.7	11.0	10.4	22
drake	0.97	0.99	0.98	0.98	13.7	20.4	14.8	24.0	16
i18s	0.04	0.40	0.40	0.52	13.0	8.4	8.7	7.9	54
i32s	0.93	0.91	0.90	0.93	7.8	10.4	9.1	8.9	89
m0e	0.99	0.99	0.99		13.8	11.0	11.7		37
m0e2afr	0.94	0.96	0.95	0.96	21.1	15.5	18.5	19.4	25
m132e	0.99	0.99	0.99	0.99	9.6	6.0	11.5	18.7	17
m30e	0.97	0.98	0.94	0.94	15.8	16.8	27.0	37.5	22
mz_n	-0.95	-0.68	0.55	0.80	25.1	16.5	10.6	8.6	5
mz_s	0.11	-0.89	-0.30	0.03	13.8	13.7	8.7	8.5	5
p10n	0.57	0.51	0.82	0.88	17.6	17.2	16.4	14.6	204
p24n	0.83	0.88	0.92	0.90	13.1	9.0	10.2	11.7	183
p43s	0.27	-0.13	0.50	0.33	13.5	16.1	6.7	6.8	58
p47n	0.51	0.44	0.65	0.61	17.0	20.5	16.2	26.7	104
ts_p43s	-0.02	0.62	0.19	0.23	15.6	11.9	7.1	6.7	13
ts_p43s	0.45	0.10	0.45		9.1	11.2	6.8		67
Mean	0.56	0.51	0.68	0.70	13.4	13.1	11.9	13.4	

Absolute mean sea surface height as inferred from TOPEX/POSEIDON (T/P), a hydrographic inversion (Hyd) [*Macdonald* 1995], and the model runs POCM_4B (4B) and POCM_4A (4A). T/P and POCM_4B field are taken from 1993/1994. The run POCM_4A represents 1988/1989. Shown are correlation coefficients and root-mean-square differences.

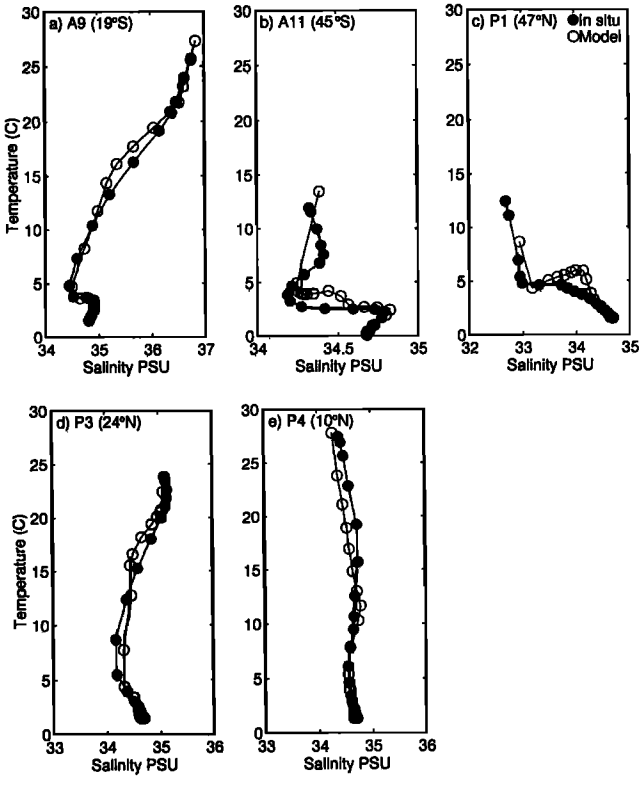

Figure 3. *T-S* diagrams from the model *T,S* fields along five WOCE lines together with observed *T,S* distribution. (a) A9, 19°S in the Atlantic, (b) A11, 45°S in the Atlantic, (c) P1, 47°N in the Pacific, (d) P3, 24°N in the Pacific, and (e) P4, 10°N in Pacific.

the Pacific Ocean and along 48°N in the North Atlantic (Figure 1f). A pronounced shift in the general circulation by about 10° zonally can be identified as a major reason for the discrepancy between the model and T/P in the latter section. Along the same section, T/P data indicate an increased geoid uncertainty in the eastern North Atlantic but do agree remarkably well with the hydrography, taking into account the smoothing of the T/P field which eliminates the sharp frontal structure of the North Atlantic Current.

The largest discrepancies between T/P results and the hydrography occur in the tropical Pacific, where the geoid estimates are known to be extremely poor [*Stammer and Wunsch*, 1994]. Here differences of more than 20 cm in amplitude are present on large spatial scales (Figure 1c), which otherwise can only be found along continental boundaries (Figure 1d) or at isolated locations such as 180° longitude in Figure 1d. The challenge of future work will be to bring all three estimates together at the centimeter level of accuracy, which on basin scale is equivalent to an uncertainty in mass transport of 7 Sv, as indicated above.

We turn now to the T and S characteristics of the model. In the present context of the large-scale ocean circulation, we concentrate on two aspects. A discussion of *T-S* characteristics along various WOCE hydrographic sections is provided here. Wavenumber spectra of temperature variability in the model and observations will be shown in section 4.5. These two comparisons show how well the model simulates (1) the mean oceanic water mass characteristics and (2) the spatial variability of ocean temperature.

Figure 2 shows observations together with the model simulation along the WOCE line A9 at 19°S in the Atlantic. This line is representative of the model's general characteristics, similarities in large-scale trends, and biases. On the large scale, the temperature fields agree very well, with isotherms rising toward the east across the Atlantic.

At depth, a close agreement between both fields is to be expected because of the long adjustment timescale of the deep model layers which prevents the model drifting away from its initial Levitus conditions. But in the upper thermocline, the adjustment of the wind-driven circulation is relatively rapid, and the model has reached, asymtotically, an equilibrium state. As a consequence, the model is too cool by about 2°C in the top 200 m of the western basin. At the depth of the 15 °C isotherm, both fields are consistent, but below this level, the model is warmer in the eastern basin.

T-S diagrams of the model and in situ data are shown in Figure 3 for all five WOCE lines. From A9 at 19°S (Figure 3a), an almost identical pair of *T-S* curves is found for the model and in situ data, meaning the model is representing the real oceanic water masses on the large scale along this latitude in the Atlantic. Similarly, we find a relatively good agreement at the other low-latitude lines P3 (24°N; Figure 3d) and P4 (10°N; Figure 3e), with the exception that along P4, the model underestimates the surface salinity owing to the lack of realistic surface salt fluxes in the simulations. To the contrary, the agreement is poor in the high latitudes. For A11 (45°S; Figure 3b) distinctively different *T-S* curves are obtained in the top 1500 m depth. The model does not produce the Subantarctic Intermediate Water (the upper salinity maximum) due to incorrect southern boundary conditions. This effect can be seen also at 20°S, where in the *T-S* curves from the A9 line the differences in the depth range between 100 m and 400 m are also associated with this water mass. The disagreement of the model and observations is even worse in the North Pacific for P1 (47°N; Figure 3c), where near-surface differences of about 5°C and 0.5 ppm occur for T and S, respectively, again resulting in wrong intermediate water mass characteristics.

3.3. Model Drift and Model Secular Changes

Although this paper is mostly about the variability of the upper ocean, primarily wind-driven circulation, we will briefly summarize the problem of model drift and secular model changes to put present results into context. The problem of model drift is a complex one, which is even more so due to various model changes which took place during the course of the 40 year integration, including surface forcing, lateral resolution, free surface, geometry, and equation of state. Moreover, the realistic forcing used in the present run makes any

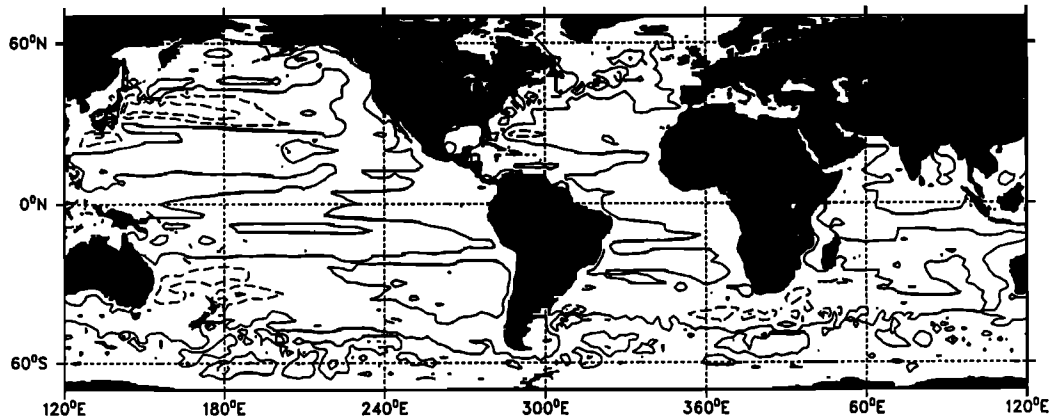

Figure 4. Differences in mean model pressure from the period 1993/1994 and 1988/1989. Contour interval is 10 cm, and first solid line is the 0 contour. Negative values are drawn by dashed contours.

analysis of model drift cumbersome, if possible at all, since it introduces long-term changes and internal oscillations in the model which are difficult to be separate from the model drift itself. An additional complication is that changes in the ECMWF model lead to discontinuities in forcing fields, which are sometimes not well documented.

A full discussion of the problem of model drift is therefore beyond the scope of this paper. A thorough discussion of influence of boundary conditions on thermohaline structures in the Community Modeling Effort is provided by *Klinck* [1995].

The model was started from *Levitus*'s [1982] initial T and S fields and integrated forward in time for about 40 years with externally specified forcing fields at the sea surface and at artificial boundaries as described previously. Because the climatology and boundary conditions contain errors and are not expected to be fully consistent with each other and the model physics, the model necessarily drifts away from the initial conditions. But due to the long timescales of the general circulation, the model equilibrates only slowly in its thermohaline deep circulation over $O(100 - 500)$ years. Even after 40 years of integration, the model global average temperature and salinity continue to drift. In the last year of the run, 1994, the near-surface temperature field is still cooling by about 0.05°C per year. This trend decreases with depth and reverses in sign at depth. The drift in near-surface salinity is of 0.01 ppm for the same period. On global average, the model cools by about 0.03°C during the first 4 years of POCM_4B but remains constant afterward. For a global average salinity drift, roughly the same picture emerges.

An understanding of long-term changes in the model is important in the context of a comparison of mean model fields with data. Figure 4 displays the difference of the mean POCM_4B SSH from the period 1993/1994 relative to a mean from the period 1988/1989. Differences in the mean SSH fields of up to 20 cm are visible, which are mainly residing in the steric (density) component of surface elevation (see section 5).

4. Variability

4.1. SSH Variability and Eddy Kinetic Energy

Comparisons of the variability fields of models and altimeters have been previously produced by *Treguier* [1992], *Stammer and Böning* [1992], *Beckmann et al.* [1994b], and *Stammer and Böning* [1996]. Altimetric variability is independent, to first order, of any geoid error. For T/P, the error component of the time varying signal is of the order of 4 cm^2 [*Fu et al.*, 1994; D. Stammer, Regional aspects of global frequency-wavenumber spectra of oceanic variability estimated from TOPEX/POSEIDON altimeter measurements, submitted to *Journal of Geophysical Research*; hereinafter referred to as Stammer, submitted manuscript, 1996a].

The rms SSH variability from both T/P and POCM results is given in Plate 2, which shows rough agreement in terms of the spatial distributions. But a closer look reveals an important difference in terms of amplitudes which is readily detectable from the general background variability in the interior oceans. There the model shows less than 50% of the observed SSH variance, even after taking the T/P errors into consideration. To facilitate a comparison, Figure 5 shows, in its left column, zonal averages of SSH variance from POCM_4B and T/P, computed separately for the Atlantic, Pacific, and Indian Oceans. At a few locations, the SSH variances in the model match zonally averaged observations, e.g., in the North Atlantic Current (Figure 5a). However, discrepancies are much larger at those locations where the model fails to produce mean frontal structures and their associated internal variability. A striking example is the Azores Front in the North Atlantic, where observed SSH variance is up to a factor of 8 larger. Similar discrepancies are located at various frontal structures in the Pacific (see Figure 5b) and in the Indian Ocean (Figure 5c). And apart from the Indian Ocean sector, the variability associated with the ACC is grossly underestimated by the model. For com-

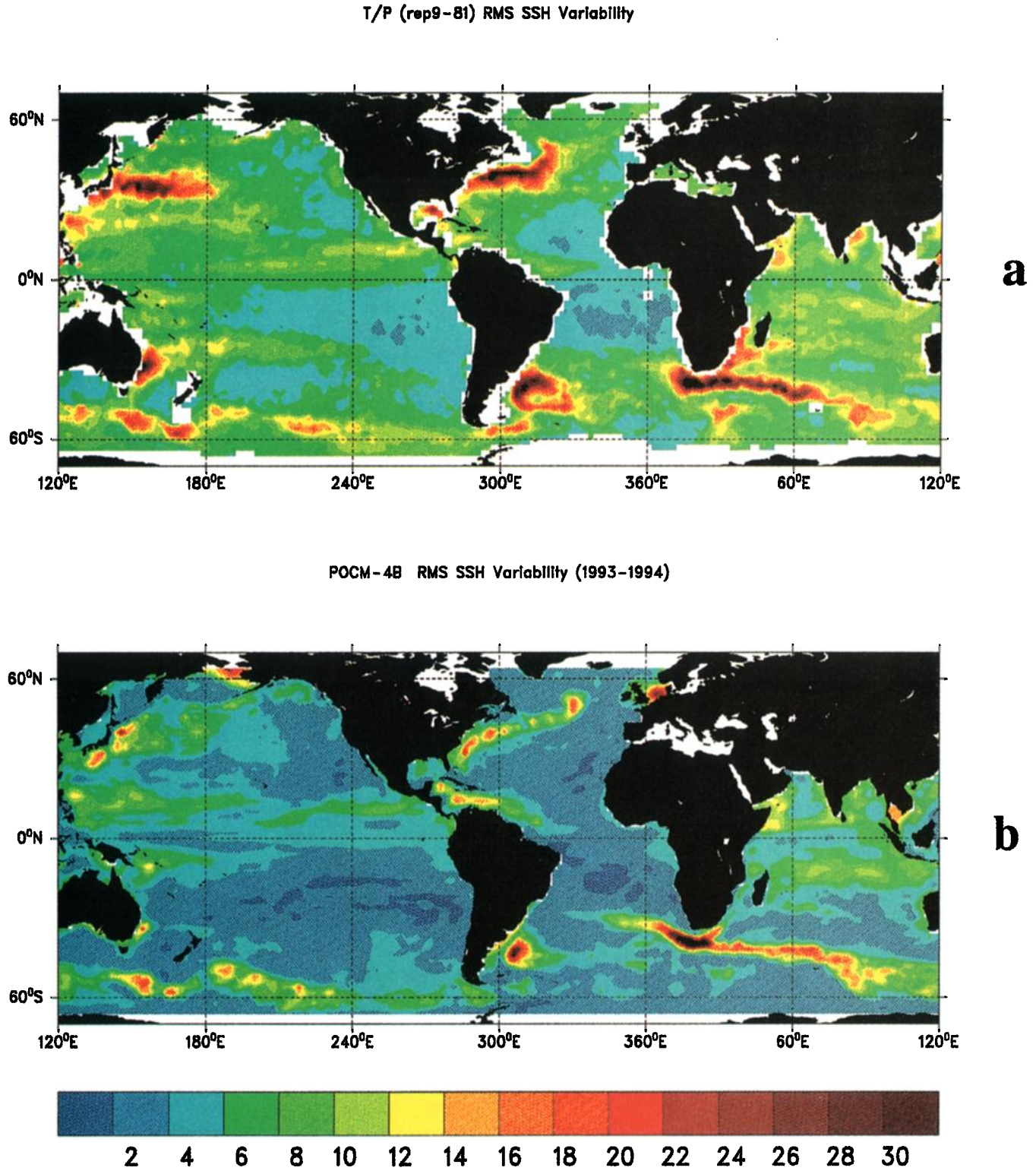

Plate 2. (a) T/P RMS sea surface height variability estimated from the 2-year period repeat 9 through 81 at each along-track position and averaged subsequently in 2° x 2° geographical areas. (b) POCM_4B RMS sea surface height variability from 2-year period 1993/1994. Contour interval is 2 cm.

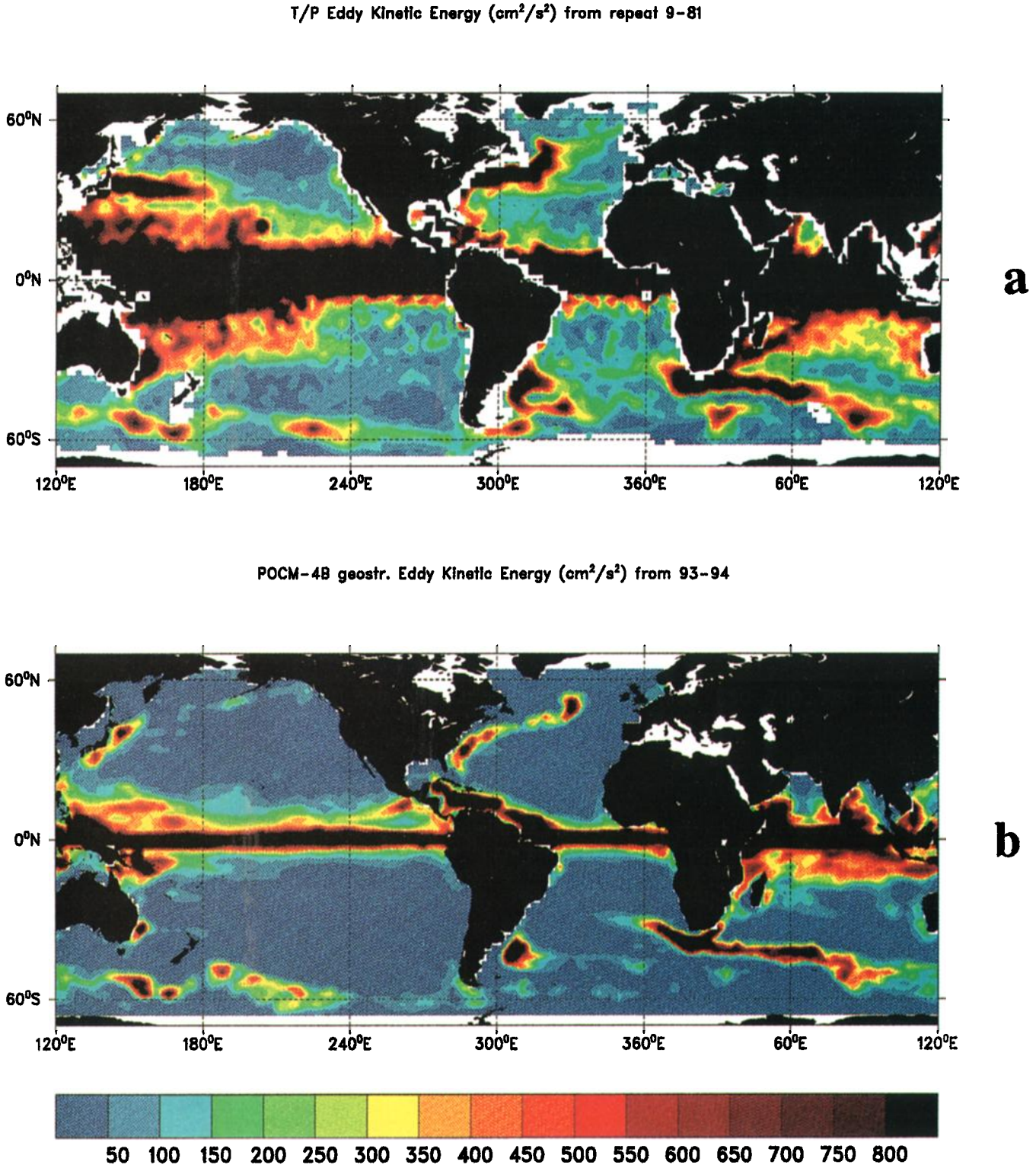

Plate 3. (a) T/P eddy kinetic energy estimated from cross-track geostrophic velocity anomalies, assuming isotropy. Data were smoothed over 30 km previously, and a remaining noise component corresponding to about 1 cm data uncertainty was corrected for. (b) POCM_4B kinetic energy of geostrophic eddies evaluated from the 2 years 1993/1994. Contour interval is 50 cm^2s^{-2}.

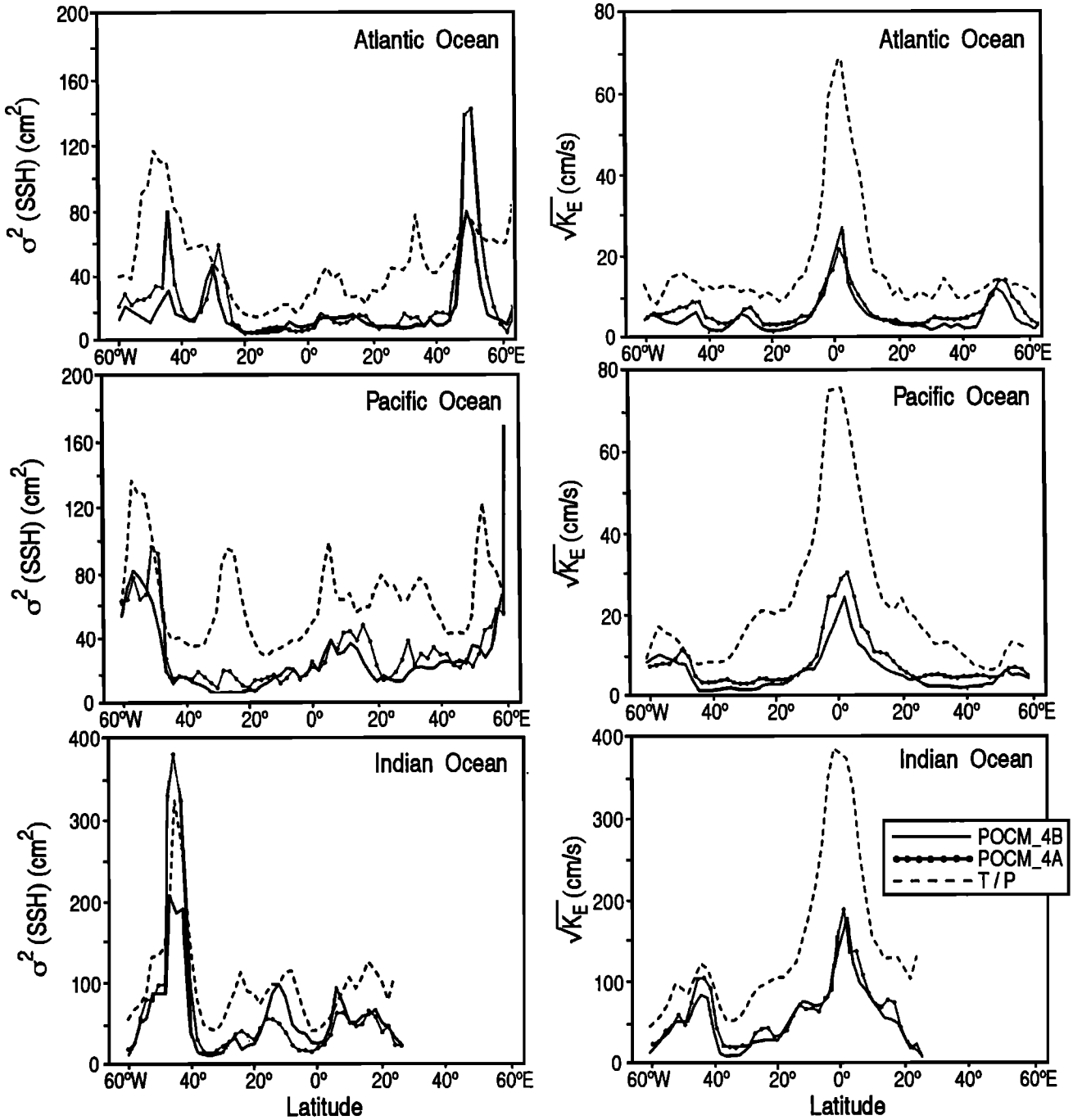

Figure 5. Zonal averages (left) of sea surface height variance (in square centimeters) and (right) of $\sqrt{K_E}$ (in centimeters per second) as a function of latitude from POCM_4B (bold solid lines) and as inferred from T/P (dashed lines). Also included in the figure are results from POCM_4A (solid-dotted lines), to illustrate effects of the changed forcing fields on the overall variability level and on local currents. Averages are obtained in the Atlantic between 30°W and 10°W, in the Pacific between 180°E and 230°E, and in the Indian Ocean between 60°E and 90°E.

parison, the figure also shows similar results, but from the previous run POCM_4A. It is clear that the recent run is less eddy active, especially in intense currents. This implies that the change from monthly wind-stress fields to daily fields does not reduce the discrepancy in model variance relative to T/P observations.

It has been shown that about 50% of the observed variance present in the T/P data resides on timescales longer than the mesoscale, i.e., longer than 150 days [*Wunsch and Stammer*, 1995]. Most of the energy on these long time scales is associated with the annual cycle in large spatial scale SSH due to sea surface buoyancy fluxes [*Pattullo et al.*, 1955; *Pattullo*, 1963; D. Stammer, Steric and wind-induced changes in large-scale sea

surface topography observed by TOPEX/POSEIDON, submitted to *Journal of Geophysical Research*; hereinafter referred to as Stammer, submitted manuscript, 1996b]. As will become more clear below, the model is not able to completely simulate this component of the variability, in part due to the lack of an appropriate parameterization of mixed layer physics. Correspondingly, a comparison of the model rms variability shows much more resemblance with the rms amplitude from high-pass-filtered T/P data (containing energy on timescales less than 150 days) both in pattern and amplitude (see Plate 4a of *Wunsch and Stammer* [1995]).

Because the steric component of SSH variability is large scale, it does not significantly affect the flow field and its influence should disappear in a field of eddy kinetic energy K_E. Plate 3 shows maps of the eddy kinetic energy

$$K_E = \frac{1}{2}(u'^2 + v'^2) \tag{2}$$

with u' and v' being fluctuations of the zonal and meridional velocity components, respectively, from POCM_4B (Plate 3b) and T/P (Plate 3a) for the period 1993/1994. Zonal averages of those fields, similar to those from SSH variance, are displayed in the right column of Figure 5. The T/P eddy kinetic energy was derived from cross-track geostrophic velocities assuming an isotropic eddy field in the ocean, after removing all energy on spatial scales smaller than 30 km and after correcting a residual noise of about 1 cm in the smoothed SSH data as described by Stammer (submitted manuscript, 1996a). In the North Atlantic along 30°W, the resulting K_E field agrees with estimates obtained from surface buoys equipped with drogues at 100-m depth [*Brügge*, 1995]. To be consistent with the T/P observations, the model eddy kinetic energy was computed geostrophically from 10-day averages of the model SSH fields.

Observed K_E field is also a factor of 2 to 4 higher in amplitude than simulated by the model (see Figures 5d, 5e, and 5f). In addition, regional deficiencies of the model in simulating observed eddy variability are readily apparent. This defect is particularly obvious in the vicinity of the equator. It is likewise apparent at various locations, where high observed variability is not represented in the model. For example, most of the observed variability associated with the Mozambique Current is missing in the model. It is noteworthy that the model feeds the Agulhas Current primarily through the Mozambique Channel, while T/P observations indicate a significant volume flux with associated variability into the Agulhas Current from the east side of Madagscar.

A well-known discrepancy between simulated and observed variability is related to the difficulty models have in simulating the extension of a high-variability tongue into the interior ocean following the path of intense currents such as the North Atlantic Current and Azores Current and the Kuroshio. Another general problem is related to the lack of local energy maxima observed at various places along frontal structures such as the ACC. Other examples of model failure are near the Southwest Indian Ridge south of Africa and in the variability associated with the Brazil-Malvinas Confluence in the western South Atlantic.

Dynamical causes responsible for the lack of model variability have been reviewed recently by *Stammer and Böning* [1996] for the North Atlantic. As discussed by them, the lack of energy in the models is partly related to deficiencies in the simulated hydrographic structures, which prevent baroclinic instability processes from serving as adequate energy sources. The same problem appears in other dynamically weak regions in the model, such as the subarctic front in the South Atlantic.

The question remains open as to what prevents the model from developing the overall background energy level away from frontal structures. One key factor is spatial resolution of the model [*Böning and Budich*, 1992; *Beckmann et al.*, 1994a]. Of at least similar importance, however, seems to be the influence of dissipation on the overall energy level, which is responsible for the pronounced energy drop on high wavenumbers [*Spall*, 1990; *Böning and Budich*, 1992], but with increasing spatial resolution a decrease in the dissipation coefficient can be accomplished [*Beckmann et al.*, 1994b]. Which of the two components is more important to increasing the overall energy levels in eddy resolving models remains unclear from those experiments.

To understand the effect of dissipation on the overall eddy energy, another effect has to be taken into account. Due to near thermal wind balance, any erosion of T and S structures in the upper layers through the effect of the surface T, S boundary condition acts as a friction term for the velocity field, with a timescale of 30 days. In a different context, a significant effect of the relaxation of T and S toward a climatology on large-scale SSH anomalies has been recognized by *Stammer and Wunsch* [1996]. Ocean observations showing, e.g., Gulf Stream rings or Agulhas eddies over the timescale of a year, suggest that a damping timescale of the mesoscale through the surface T, S boundary condition of the order of 30 days is much too short and a scale dependent damping seems to be required. Related studies have been performed recently by *Xu et al.* [1995], who found an increase in eddy energy of more than a factor of 2 (locally) with a surface temperature boundary condition chosen according to *Rahmsdorf and Willebrand* [1995]. *Spall* [1990] estimated the dissipation of eddy energy due to a surface T, S boundary relaxation condition of the same order as interior basin energy production through baroclinic instability. Preliminary experiments with the present model with doubled relaxation timescale, γ, did not lead to any noticeable increase in eddy energy, however. Whether the wind-stress estimates being used are accurate to a factor of 2 in energy level is likewise not entirely clear.

If processes such as friction, or systematic wind-stress errors, can be considered responsible for the general lack of model variability, the ratios of variability from various parts of the ocean could still roughly reflect the observed ratios. This, indeed, is the case, as shown in

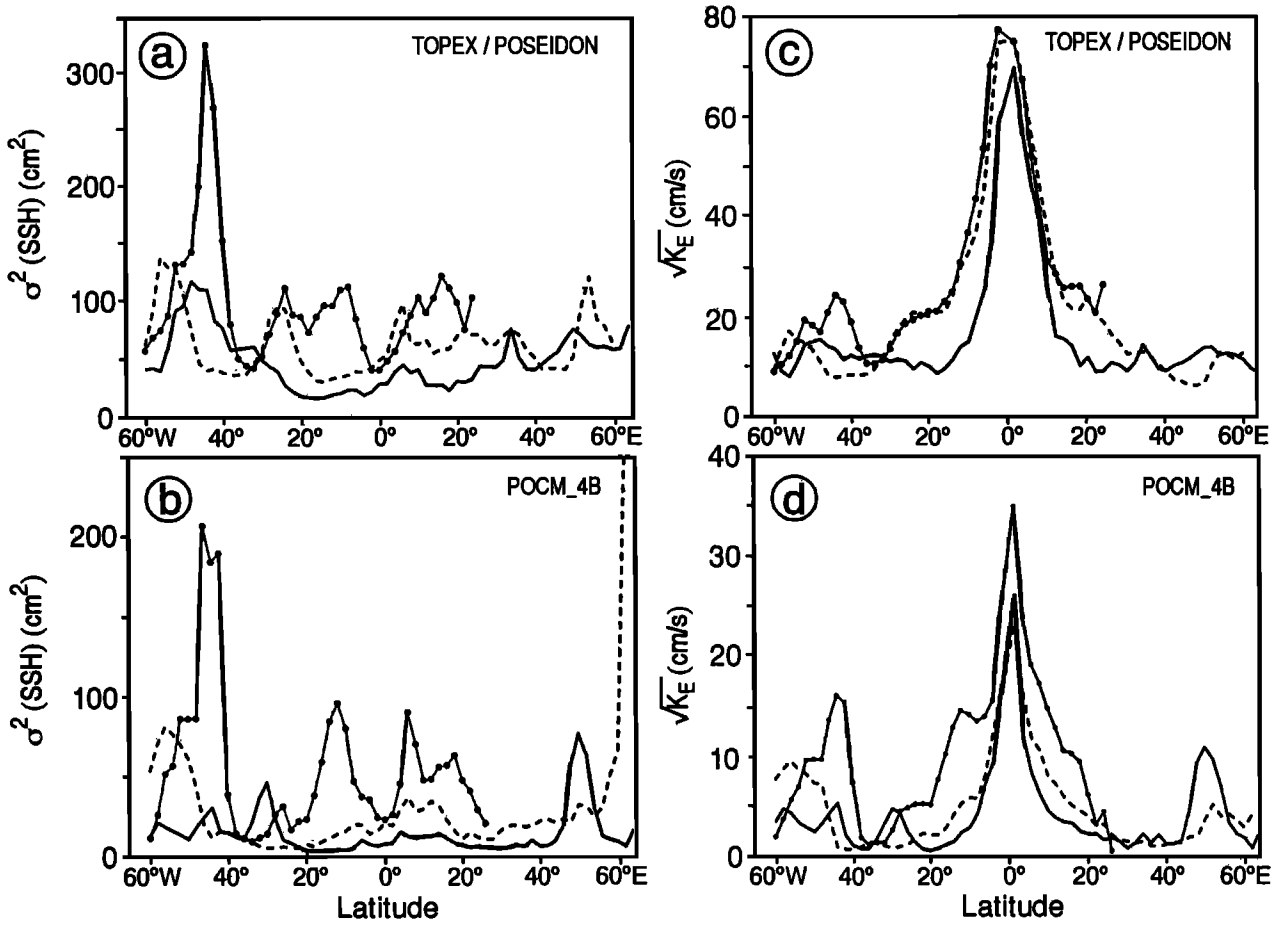

Figure 6. (a) Zonal averages of sea surface height variance (in square centimeters) as a function of latitude obtained from T/P during 1993/1994 in the Atlantic between 30°W and 10°W (solid line), in the Pacific between 180°E and 230°E (dashed line), and in the Indian Ocean between 60°E and 90°E (solid-dotted line). (b) same as in Figure 6a, but from POCM_4B. (c) Zonal averages of $\sqrt{K_E}$ (in centimeters per second) as a function of latitude inferred from T/P for the same zonal ranges as in Figure 6a. (d) same as Figure 6c, but from POCM_4B.

Figure 6, comparing zonal averages of SSH variance and $\sqrt{K_E}$ taken from the central basins of all three oceans with each other, separately for T/P and POCM_4B. Note that generally maximum SSH variance and eddy kinetic energy are found in the Indian Ocean, whereas the Atlantic appears quietest. Most locations of high and low variability in the model and their relative amplitudes are simulated successfully by the model. Except near the missing frontal structures, the relative amplitudes of variability in different oceans or along the ACC are found to be similar. The increase of K_E from high to low latitudes also appears with roughly the same ratio as observed (in particular in the Indian Ocean, but note the different vertical scale), giving confidence also in the K_E estimates from T/P in low latitudes.

The fact that the model variability deviates from observations in low latitudes, where the first-mode deformation radius is well resolved, as much as in high latitudes, is counterintuitive. But one has to recall that the friction and diffusivity in the model are weighted by $\cos^{2.25}(\phi)$ and it is likely that this is the reason why high latitudes do well in spite of small deformation radii. This finding lends strong support to the hypothesis that to first order the model friction rather then resolution is controlling simulated energy levels.

4.2. Drake Passage Transport Fluctuations

The Drake Passage transport is one of the better measured Southern Ocean regions. An estimate of the mean model transport is 163 Sv (P. Challenor and R. Tokmakian, Monitoring Drake Passage transport from altimetric data, unpublished manuscript, 1996). This number is still high, but closer to estimates of about 124 Sv from an array of current meter moorings provided by *Nowlin et al.* [1977] than those obtained from POCM_4A (196 Sv). A thorough discussion of various different estimates of mean transport through the Drake Passage is provided by *Peterson* [1988] and *Peterson and Stramma* [1991].

The precision of T/P permits monitoring of Drake Passage transport fluctuations which are otherwise not easily measurable. We compare in Figure 7a model transport fluctuations through the Drake Passage (solid line) with those from T/P (dashed line) inferred from

cross-straight SSH differences. Transports are assumed to be proportional to the cross-strait height difference and have be computed by invoking geostrophy and by assuming a velocity profile decreasing linearly with depth over a wedge-type strait. Results from T/P indicate transport fluctuations of roughly ± 10 Sv which are consistent with those from a moored current meter array [*Whitworth*, 1983]. The model indicates only half of that value and completely lacks resemblance with T/P estimates. Similarly low model transport fluctuations follow likewise from direct estimates (P. Challenor and R. Tokmakian, unpublished manuscript, 1996). A lack of resemblance between the model and T/P observations follows also from the time series of SSH at either end of the section (Figures 7b and 7c). *Woodworth et al.* [1996] report SSH fluctuations both from T/P and in situ data which are consistent with T/P estimates given in Figure 7b at the northern side of the Drake Passage (57.8°S).

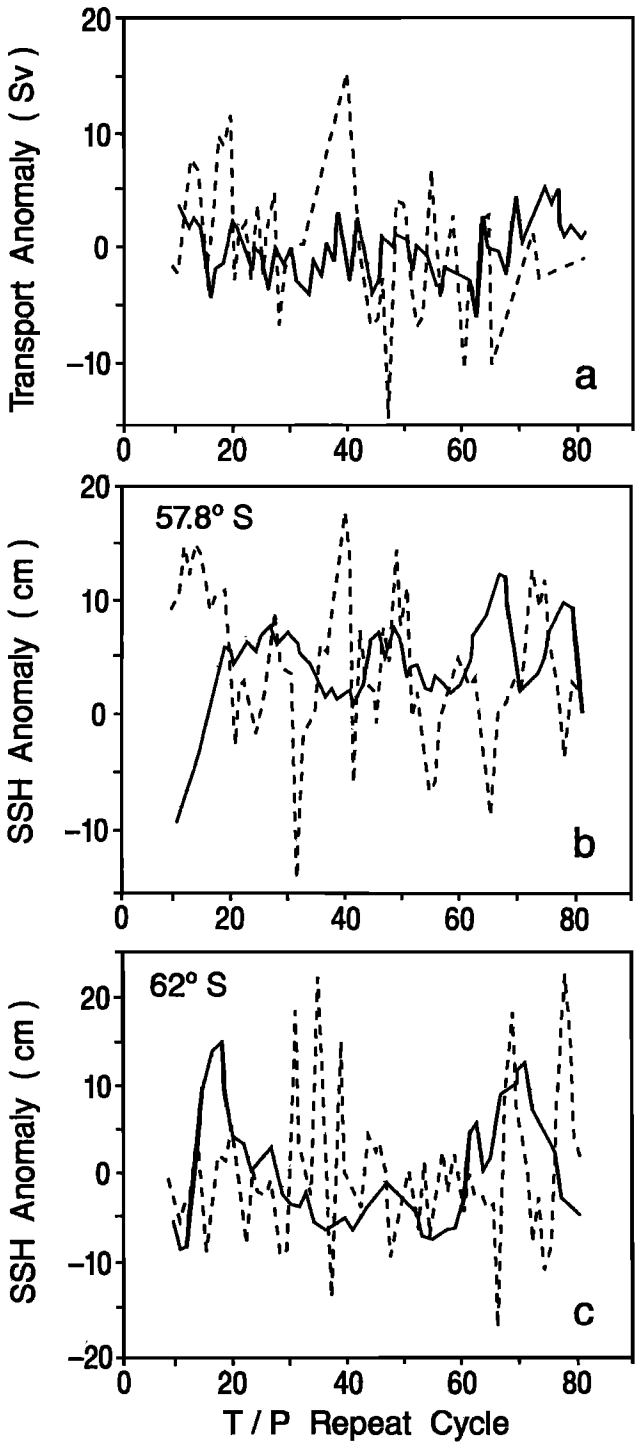

Figure 7. (a) Drake Passage transport variations relative to 2-year mean estimated from cross-strait sea surface height gradient (see text) from POCM_4B (solid line) and T/P fields (dashed line) every 10 days. The sea surface height variation from both fields at the northern and southern end of the cross-strait section at (b) 57.8°S and (c) 62°S.

Wearn et al. [1980] and *Whitworth* [1983] show that transport fluctuations through the Drake Passage are largely controlled by fluctuations in the wind stress. To the extent that SSH changes across the strait are indicative of transport fluctuations, we conclude that either the wind-stress of the ECMWF model is extremely poor over the Southern Ocean or that there are other physical factors involved which are not sufficiently represented by the model. From a comparison of model data with tide gauge observations, R. Tokmakian (Global ocean models reproduce climatic sea level fluctuations, unpublished manuscript, 1996) concluded that ECMWF products have reduced skill in the South Pacific as compared to other parts of the world ocean.

4.3. SSH Frequency-Wavenumber Spectra

In a recent paper, *Wunsch and Stammer* [1995] studied the global variability of the ocean from 2 years of T/P data. Two-dimensional frequency-wavenumber spectra are provided as global averages on timescales larger than the nominal "10-day" repeat cycle of T/P (more exactly, 9.91 days) and on spatial wavenumber between roughly 10 km (the along-track Nyquist wavelength) and 40,000 km. Global averages such as these are a fundamental element in describing the ocean circulation and its variability and provide a useful summary.

The SSH fields obtained from POCM_4B have been analyzed in a similar manner to that done with T/P maps: instantaneous model fields stored every 3 days were averaged over the T/P repeat periods for repeat cycle 9 through 81 on a 2° by 2° grid, and the resulting fields were expanded into spherical harmonics. The globally averaged frequency-wavenumber spectrum is obtained from the time series of individual harmonic coefficients. The spectrum was computed by taking the coefficients of the spherical harmonic analysis in time and Fourier analyzing them to produce $|\hat{\alpha}_{n,m}(\sigma)|$. These in turn were summed over the orders $m = -n$ to n to produce the so-called degree variances as a function of frequency σ. The result was then transformed, as described by *Wunsch and Stammer* [1995], into a one-dimensional wavenumber spectrum, equivalent to that which would be obtained as a global average along-track spectrum if one had data along all possible great circles. An analysis of regional frequency and wavenumber spectra from T/P data is provided by Stammer (submit-

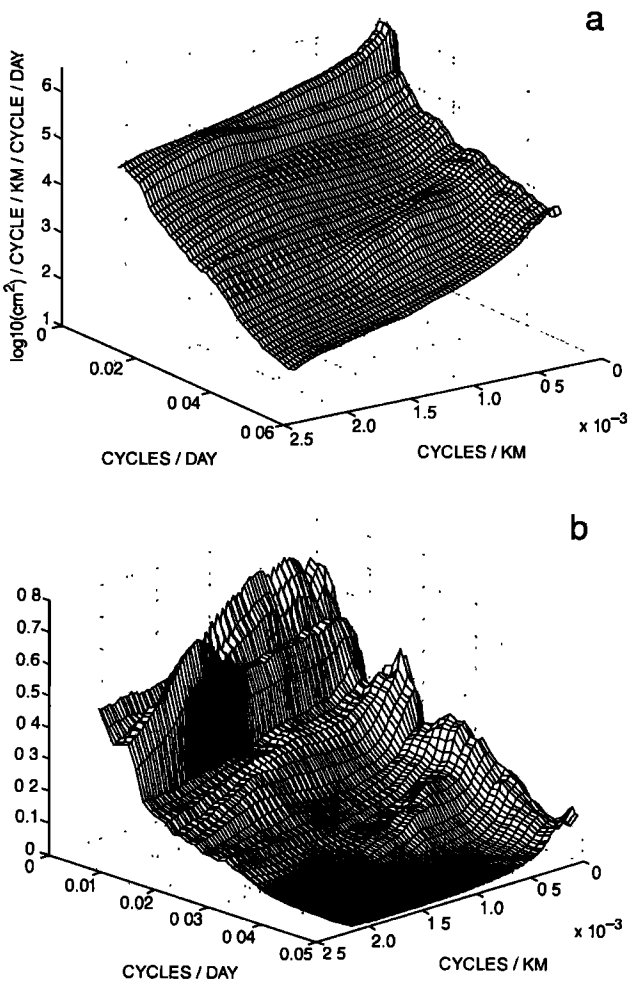

Figure 8. (a) Frequency-wavenumber spectrum of the model sea surface height. (b) The ratio of simulated energy relative to similar T/P results. See text.

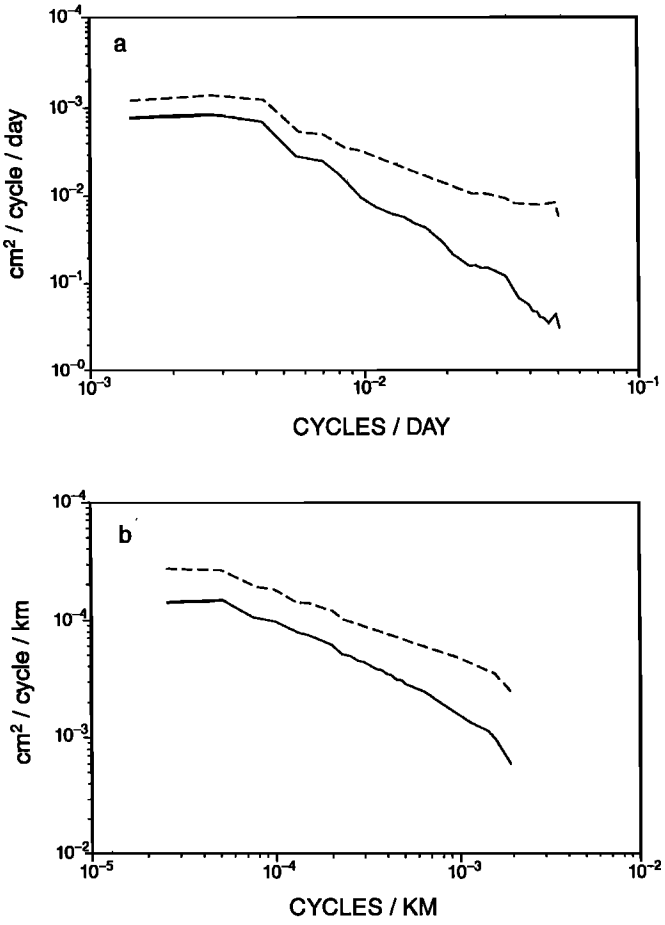

Figure 9. (a) Frequency spectra from POCM_4B (solid line) and T/P (dashed line) and (b) corresponding wavenumber spectra, both obtained by summing over all wavenumbers and frequencies in the frequency/wavenumber spectra.

ted manuscript 1996a) and a comparison of T/P results with 1/4° and 1/6° OGCMs is given by McClean et al. (submitted manuscript, 1996).

A resulting frequency-wavenumber spectrum is shown in Figure 8a, characterizing SSH variability from POCM_4B on wavelengths longer then 450 km for the period 1993/1994. The spectrum, which was smoothed over three neighboring frequencies and three neighboring wavenumbers, should be be compared to Figure 2b of *Wunsch and Stammer* [1995] (note the vertical axis is mislabeled there). The ratio of the model power relative to the observed one, is shown in Figure 8b. Separate frequency and wavenumber spectra which result from summing over all wavenumbers or frequencies, respectively, are shown in Figure 9, for both the model and T/P.

Model energies are clearly too low at all frequencies and wavenumbers with a notable failure at high frequencies and wavenumbers. On a timescale less than about a month and on spatial scales below 1500 km, the model simulates only a small fraction (< 10%) of the variability present in T/P data. Toward long scales both in space and time, discrepancies are reduced to about 50%.

At two locations in frequency-wavenumber space, the model indicates a slight increase of energy above the general behavior. The first is located on timescales between 140 and 175 days and spatial scales shorter than about 600 km and is most likely associated with the mesoscale activity of high-energy areas such as boundary currents or the ACC. The other region occurs on timescales and space scales of about 25 days and spatial scales between 1000 and 2000 km. The close agreement of those scales with the barotropic radius of deformation, and the short timescales are very suggestive that we are seeing the energy of high-latitude barotropic Rossby waves enhanced by high-frequency wind-stress fluctuations [*Fu and Davidson*, 1995; *Fu and Smith*, 1996].

The factor of 2 difference in energy at the longest periods is clearly seen in Figure 9a. Toward higher frequencies, model-data discrepancies increase systematically. At periods of 25 days the model shows a pronounced break in energy, which is not observed by T/P.

The deficit in variability is likewise documented in the wavenumber spectra (Figure 9b) which show a factor of about 2 on wavelength longer 500 km and a faster decrease in model energy on smaller wavelength.

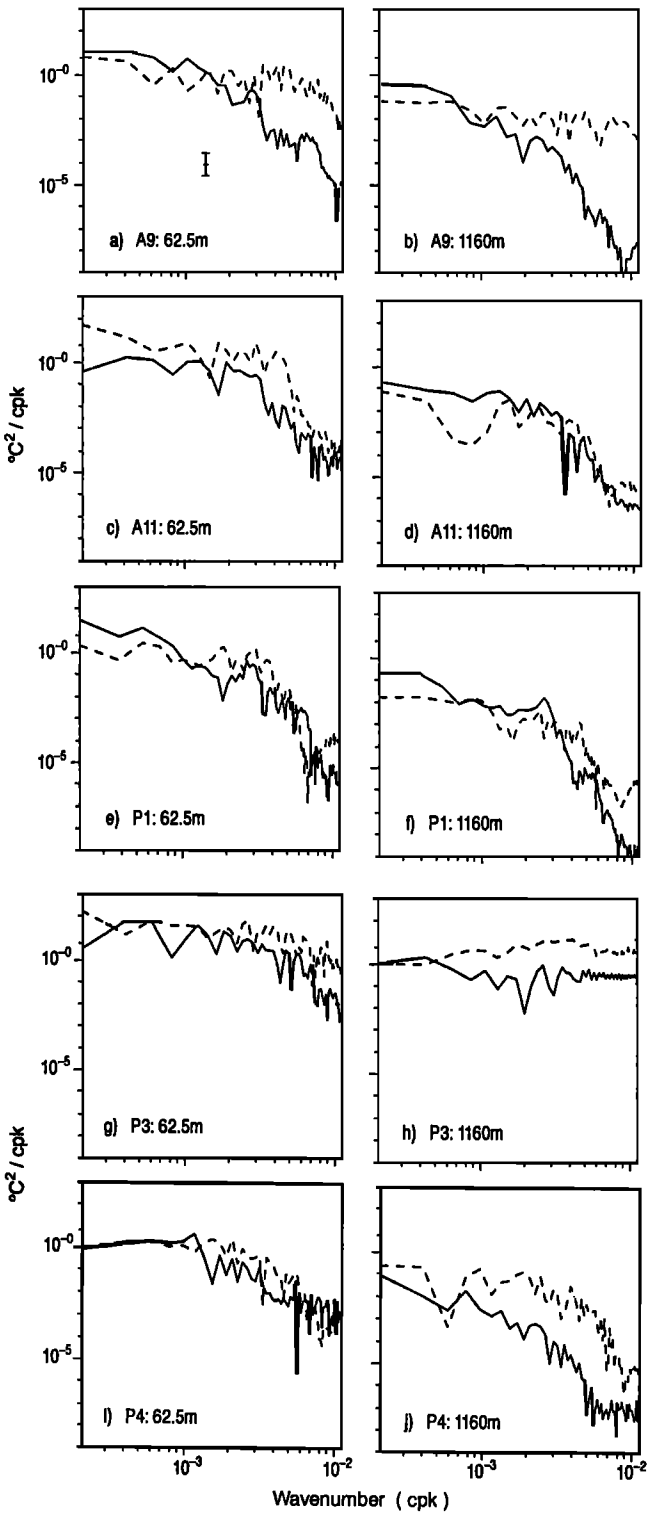

Figure 10. (a–j) Wavenumber spectra of temperature, simulated (solid) and observed (dashed), in (left) 62.5 m and (right) 1160 m depth along the same five WOCE lines as in Figure 5.

4.4. Temperature Spectra

A comparison of wavenumber spectra for in situ temperature is shown in Figure 10. The spectra are computed from the temperatures on five WOCE lines at 62.5 m (model level 3) and 1160 m (model level 12). The in situ data were fit with a spline and interpolated to the grid points of the model. The model represents the large-scale (> 400 km) temperature variability qualitatively, but at low latitudes (Figures 10a and 10b from WOCE line A9 at 19°S), the model grossly underestimates observed levels in temperature variability on wavelengths smaller than 400 km in both layers and worsens with depth. This difficulty is likely related to the 2/5° resolution zonally, as well as the increased friction/diffusivity in low latitudes. In contrast, the model successfully simulates observed variability at high latitudes where friction and diffusivity are low.

4.5. EOF Analysis

Representation of SSH fields through empirical orthogonal functions (EOFs) is complementary to a global spectral description. The advantage of the EOFs is that they allow a comparison of spatial structures of different modes and their variability in time, both of which are hidden in the global spectral description.

Global EOFs were computed from the POCM_4B and the T/P fields both provided on the same 2° by 2° grid every 10 days over the identical time span corresponding to repeat cycles 2 to 83. To do so, column vectors of time series ζ_j were constructed at each grid point, j, where T/P or model data exist, with the column vectors from all N time series forming the matrix

$$\mathbf{A} = \{\zeta_1, \zeta_2, \cdots, \zeta_N\}, \tag{3}$$

As outlined by *Fukumori and Wunsch* [1991], we computed EOFs from a singular value decomposition of $\mathbf{A}$ (see, e.g., *Jolliffe* [1986])

$$\mathbf{A} = \mathbf{U}\Lambda\mathbf{V}^T. \tag{4}$$

The singular values, $\lambda_i = \Lambda_{ii}$, which measure the strength of each mode, are displayed in Figure 11 for the model and T/P, respectively. The lack of model energy is apparent in all modes, except mode 0 which nearly corresponds to the time average.

But apart from the differences in energy, many striking similarities are present in both time and space singular vectors $\mathbf{u}_i$, $\mathbf{v}_i$. Figure 12 illustrates the time vector, $\mathbf{v}_0$, of the gravest mode. This "space mean" mode is slightly oscillatory in time in an almost identical manner for both the model and T/P fields. The meaning of this oscillation is that ridges and troughs in the spatial mode 0 pattern exhibit a similar slight pulsation in amplitude, which should not be confused with changes in global average sea level. It is noteworthy that the similarity is found over the full period of repeat cycles 2 though 83 with no degradation of the T/P data during the first eight repeat cycles (the T/P Project has suggested problems during that period [see *Fu et al.*,

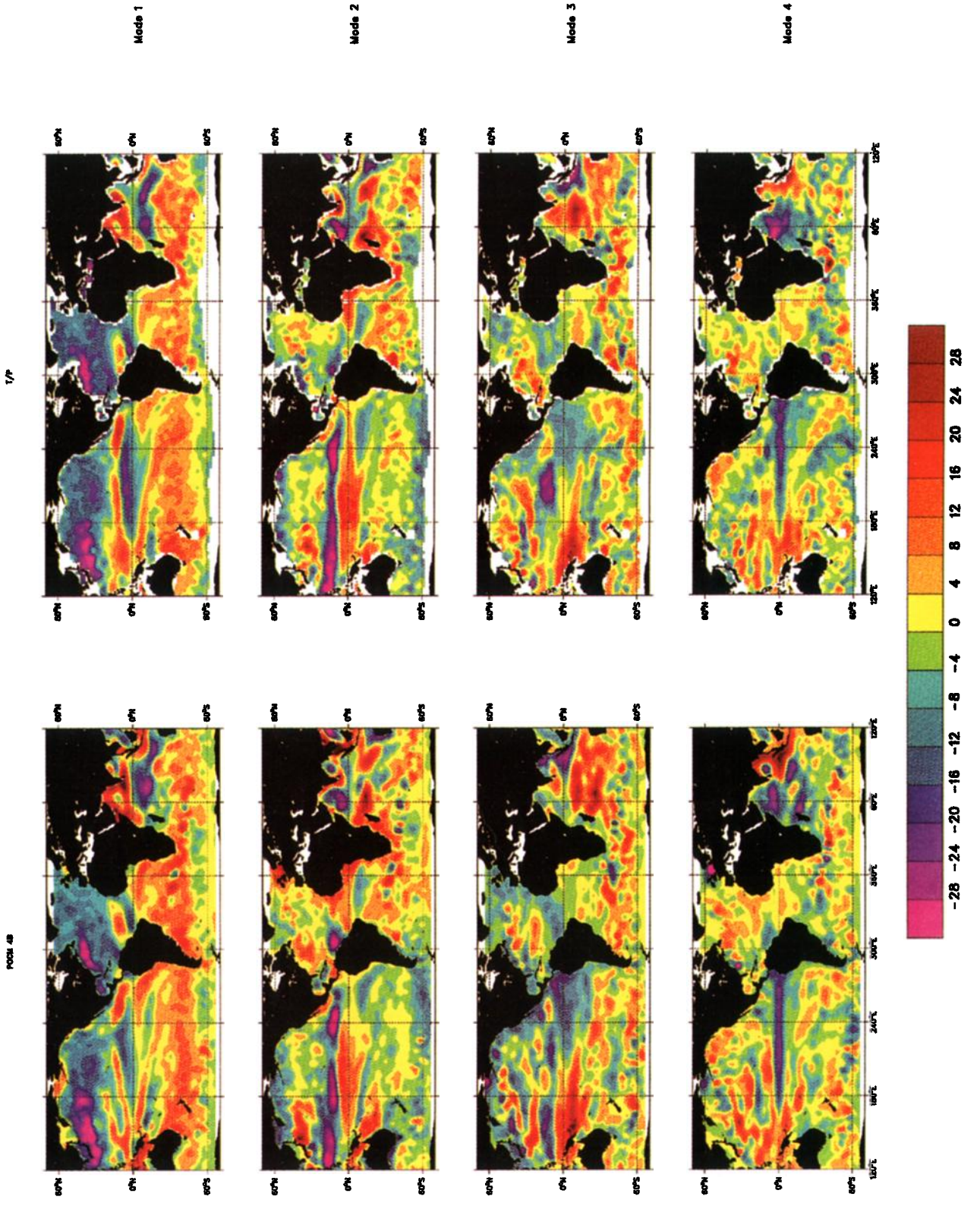

Plate 4. Spatial empirical orthogonal functions (EOFs) mode 1 through 8 from (left) POCM_4B and (right) T/P.

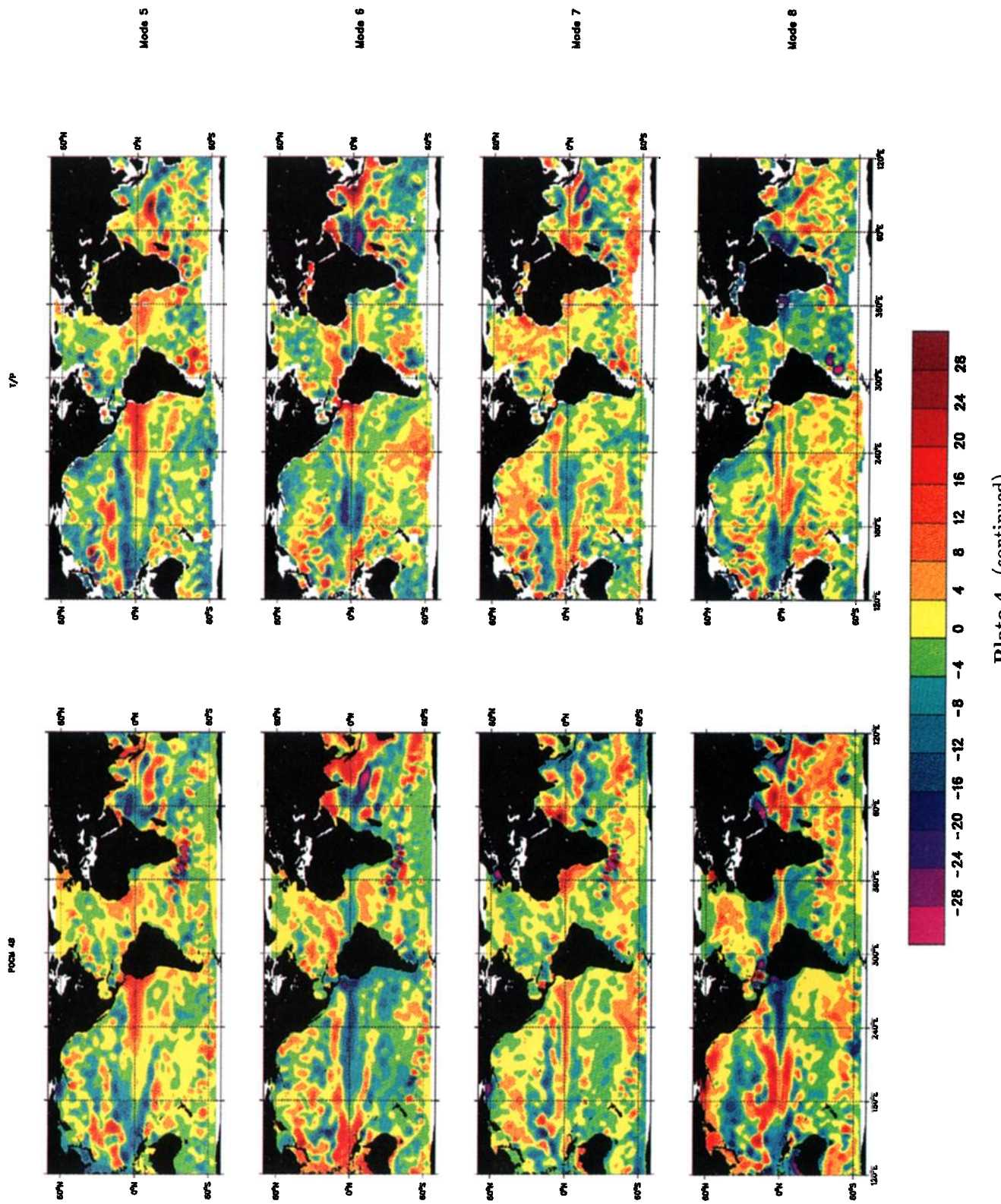

Plate 4. (continued)

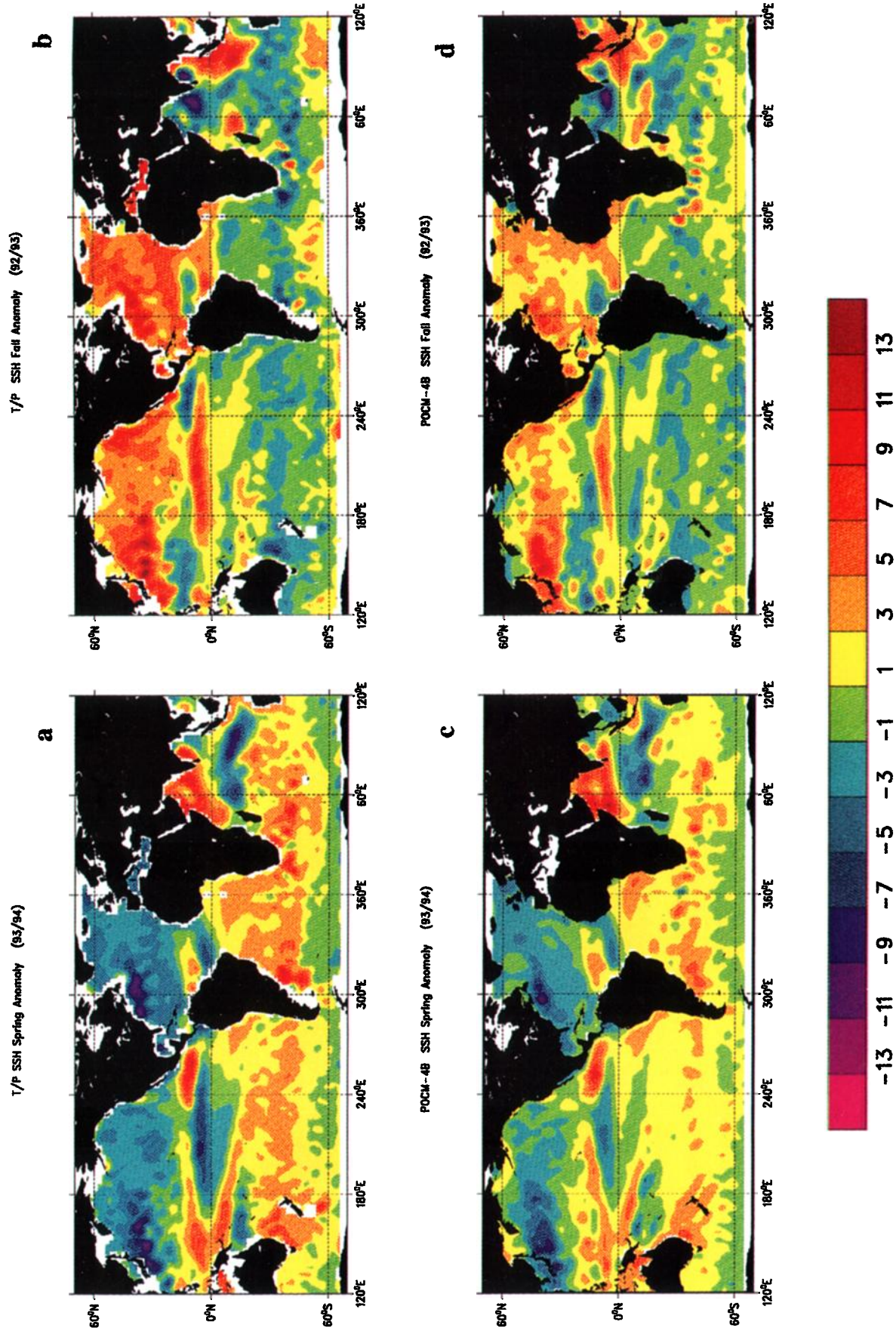

Plate 5. TOPEX/POSEIDON seasonal sea surface height anomaly from boreal (a) spring and (b) fall. POCM_4B sea surface height anomaly from boreal (c) spring and (d) fall. Contour interval is 2 cm.

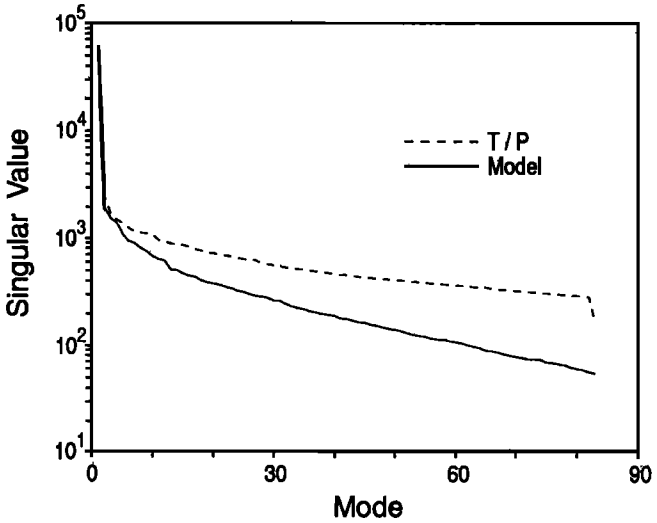

Figure 11. Singular value distribution from POCM_4B (solid line) and T/P (dashed line).

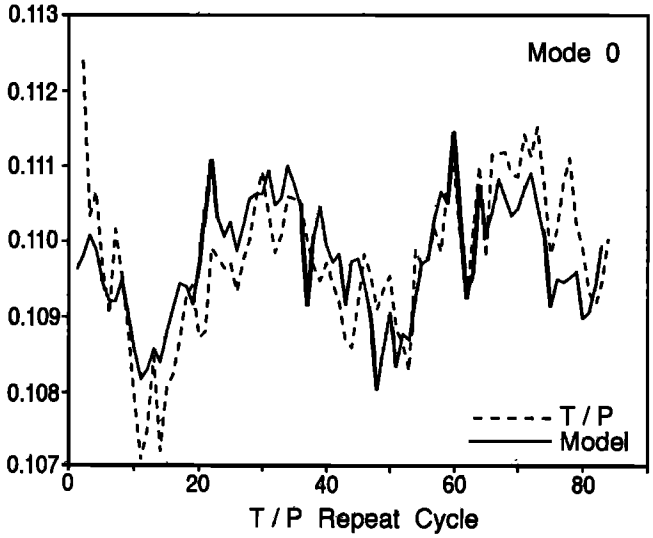

Figure 12. Mode 0 time series from POCM_4B (solid line) and TOPEX/POSEIDON (dashed line).

1994]). A comparison of time series of modes 1 through 16 is given in Figure 13. The corresponding spatial vectors $\mathbf{u}_i$, are displayed in Plate 4 for modes 1 through 8. A striking similarity is found both spatially and in time for many of the lowest modes. Although for higher modes a phase shift is found in places, the timescales are still very similar.

The modes are usually found in pairs with a 90° phase shift in time, corresponding to traveling structures. A clear example can be found in modes 1 and 2, being related to the annual cycle in sea level (compare with Plate 6). The El Niño-Southern Oscillation (ENSO) cycle is represented by modes 3 and 4, with some shorter period signals superimposed. The spatial pattern shows the west to east change in sea level in the tropical Pacific and Indian Ocean. It also includes the related response of the ocean in mid- and high latitudes visible as westward traveling Rossby waves (see also Stammer, submitted manuscript, 1996b).

With increasing mode number, increasing eddy signal is picked up. Because of the varying energy ratios, the labeling of the higher modes can be interchanged from model to T/P. For example, the spatial pattern of mode 6 in the model Pacific is similar to T/P results of mode 7, while T/P mode 6 is showing similar structures but opposite phase than model mode 8, again in the tropical Pacific.

In summary, the model successfully simulates the large-scale ocean fluctuation both in space and time. The chief issue remains the comparatively weak amplitudes.

5. The Seasonal Cycle

We now turn to a comparison of a specific phenomenon: the seasonal cycles in the model and the data. An evaluation of the seasonal cycle in the T/P observations and its close relation to local sea surface heat fluxes is described by Stammer (submitted manuscript, 1996b). It was shown by *Stammer and Wunsch* [1994] that T/P results do agree with those estimated from hydrography for the interior ocean by *Gill and Niiler* [1973] to about 1 cm. To illustrate the amplitude of the seasonal cycle as present in the T/P SSH observations and as simulated by POCM_4B, Plate 5 shows seasonal anomalies estimated from 2 years (1993/1994) of data averaged over spring (March through June) and fall (September through November), respectively. Remarkable agreement is obtained between the estimates, especially in the predominantly wind-driven tropical regime and in the Indian Ocean, where most of the structures present in the T/P fields are simulated by the model, both qualitatively and quantitatively. For example, the ridge-trough system associated with the seasonal reversal of the tropical current systems is successfully reproduced by the model with similar amplitudes and geographical locations of extreme values. Note also the strong similarity in the Indian Ocean north of 30°S. The comparison presented here is done for identical time intervals and so both fields capture ENSO events to the same degree.

A somewhat less accurate, but still surprisingly close, agreement is found in mid- and high latitudes. Many of the large-scale seasonal anomalies observed by T/P are actually present in the model fields. Amplitudes are, however, too small by about a factor of 2 in the northern hemisphere (Figure 14). Although the amplitudes of the seasonal cycle are about right in the southern hemisphere, there is a phase shift present between model simulations and T/P observations. It can be seen from Plate 6, showing both amplitudes and phases of the annual harmonic, estimated from T/P and POCM_4B maps, respectively, that the model leads the observations by about 1 month poleward of 20° latitude (compare Table 3). The reason for this peculiarity is unknown. It is noteworthy, though, that a similar

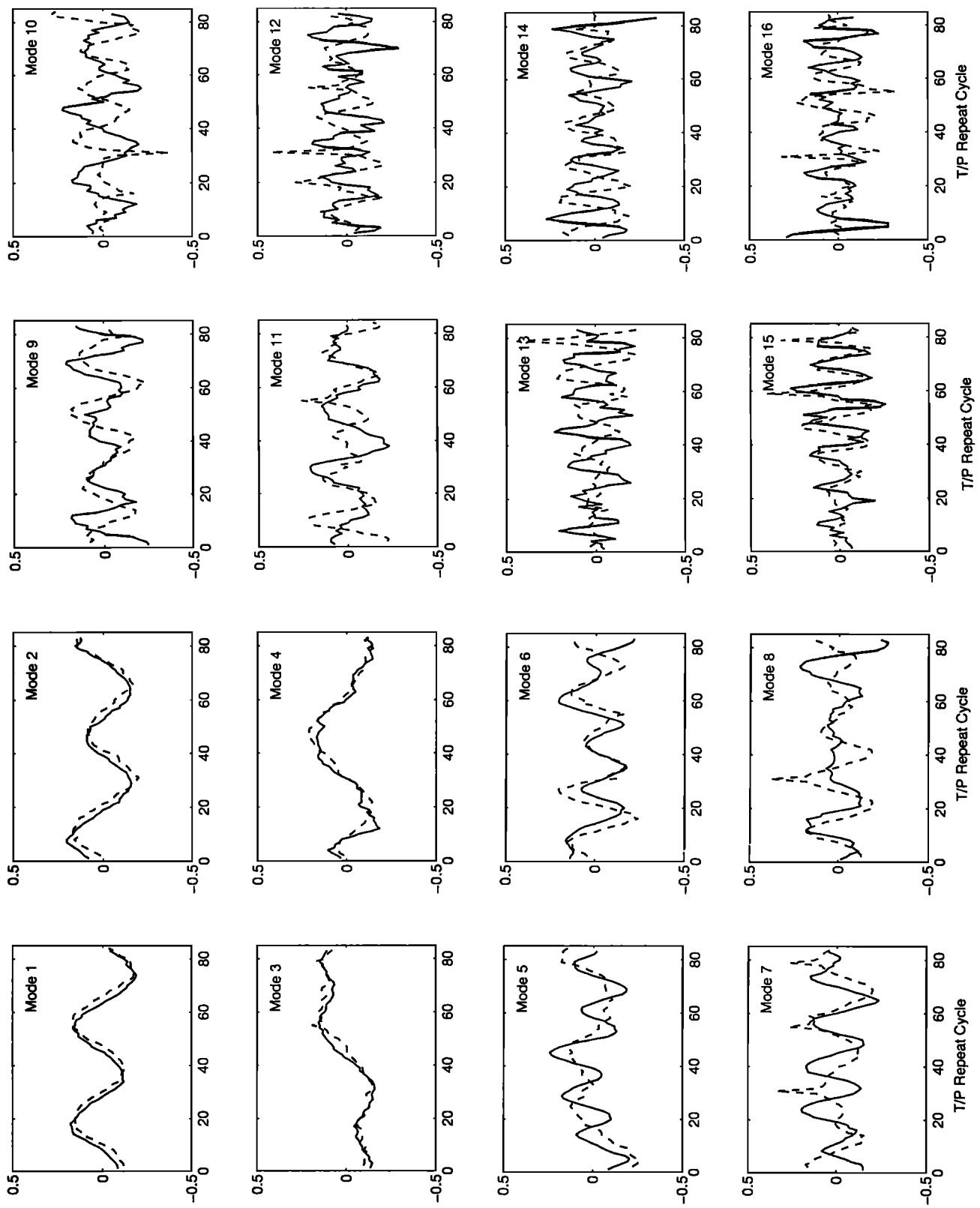

Figure 13. Time series of mode 1 through mode 16 from POCM_4B (solid line) and TOPEX/POSEIDON (dashed line).

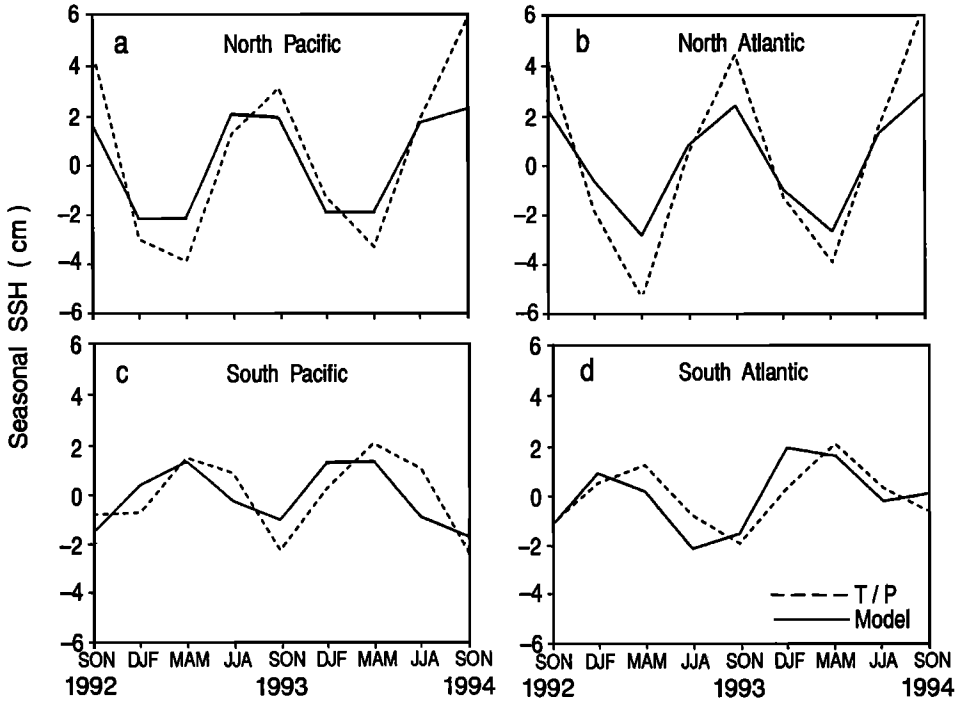

Figure 14. Basin wide averages of seasonal sea surface height anomalies from POCM_4B (solid line) and T/P (dashed line), as a function of time for the period fall 1992 to fall 1994. Fields were averaged over the area (a) 120°– 260°E, 20°– 60°N in the North Pacific, (b) 0°– 80°W, 20°– 60°N in the North Atlantic, (c) 150°– 290°E, 20°– 60°S in the South Pacific, and (d) 0°– 60°W, 20°– 60°S in the South Atlantic.

phase shift, which is most pronounced in the Pacific sector of the southern hemisphere, was obtained recently when modeling steric height anomalies by ECMWF sea surface heat fluxes (Stammer, submitted manuscript, 1996b). The coherent findings from both independent studies suggest that ECMWF heat fluxes are out of phase with observations and that T/P observations might in turn be used to correct those deficiencies of the atmospheric model.

Despite observed differences, it is worth stressing the otherwise remarkably close agreement in the annual harmonic both in amplitude and phase obtained from T/P and the model. A similar agreement could not be obtained previously from POCM_4A, which used only a simple Haney surface boundary condition for T and S and the 1980s *Levitus* [1982] surface temperature and salinity fields. Instead, model amplitudes and phases basically showed an agreement only with the purely wind-driven component in the T/P results (Stammer, submitted manuscript, 1996b).

But differences are still present, and we turn now to possible explanations for the lack of model energy in the annual cycle. A related question concerns the validity of a Boussinesq model as discussed by *Greatbatch* [1994]. According to his discussion, the present OGCM with a volume-conserving approximation captures sterically induced expansions of the water column, up to a global spatial constant, but one that varies with time. Although this missing constant can cause problems in regional model simulations, no serious effect is expected during global simulations. Similar conclusions were drawn by *Mellor and Ezer* [1995].

As discussed in detail by *Gill and Niiler* [1973], the time-varying component of the sea surface height (corrected for the effect of atmospheric loading) can be written as a sum of three terms:

$$\eta' = \eta'_s + \eta'_{bc} + \frac{1}{g\rho_0} p'_b, \tag{5}$$

where the upper layer steric anomaly

$$\eta'_s = \frac{1}{\rho_0} \int_{-h}^{0} \rho'(z) dz \tag{6}$$

is by far the dominant term on large scale outside the tropics. The depth, -h, indicates the base of the seasonal thermocline, taken to be -200 m by *Gill and Niiler* [1973]. The lower layer steric term

$$\eta'_{bc} = \frac{1}{\rho_0} \int_{-H}^{-h} \rho'(z) dz \tag{7}$$

represents the effect of expansion due to density changes below the seasonal thermocline. Those are predominantly related to mesoscale fluctuations or to changes in the vertical Ekman pumping velocity w_{EK}. The last term represents barotropic fluctuations

$$\eta'_{bt} = \frac{1}{g\rho_0} p'_b, \tag{8}$$

Table 3. Comparison of Amplitude and Phase of Annual Harmonic From T/P and POCM_4B

	POCM_4B		T/P	
Area	Amplitude	Phase	Amplitude	Phase
NP	3.0	235	4.7	262
NA	2.3	273	5.3	287
SP	2.0	100	2.9	128
SA	3.5	77	3.7	105
IO	2.6	135	3.5	135

Areas are as follows: NP, 180°– 260°E, 20°– 40°N; NA, 0°– 30°W, 20°– 40°N; SP, 180°– 290°E, 20°– 40°S; SA, 0°– 60°W, 20°– 40°S; IO, 50°– 110°E, 20°– 40°S.

in the sense of a dynamically linear, flat-bottom ocean.

Model fields permit investigation of SSH fluctuations in terms of contributions according in (5). We have used monthly mean T and S fields to evaluate the first and second term on the right-hand side of (5) with $h = -185$ m and averaged over 5° by 5° areas to focus on large scales. Subtraction of the two density terms from the total model SSH fields then leads to an estimate of the model barotropic contribution.

Amplitudes and spatial scales of the resulting fields are illustrated in Plate 7, showing all terms of (5) obtained during March 1993. While there is significant eddy structure present in the η'_{bc} field, both η'_s and η'_{bt} are predominantly large scale and of comparable, but geographically distinct amplitudes. Significant contributions of η'_{bt} to the monthly mean SSH anomalies are only present in high latitudes along the ACC and in the North Pacific. A striking exception of this tendency is found in the Indian Ocean, where enhanced barotropic fluctuations are also visible.

A decomposition of the seasonally averaged SSH anomalies of the model given in Figure 14 into the three above components is shown in Figure 15 for the same geographical areas as before. It follows that on the basin average, the η'_{bc} term is basically negligible and that η'_s is explaining most of the observed amplitude of the seasonal SSH anomalies. A phase shift between the SSH anomalies and η'_s is due to the contribution of η'_{bt} with surprisingly large amplitudes and a conspicuous large-scale pattern. The averaged barotropic term in the North Pacific is in phase with the South Pacific, but out of phase with the Atlantic Ocean. It appears to give rise to long-period interbasin oscillations on the seasonal timescale. Although small in amplitude, the η'_{bc} term still contains important information about long-term climate drifts of the model. It can be seen that the Atlantic is rising by about 0.5 cm over the 2-year time period due to associated density changes and that the South Pacific is falling slightly. The Indian Ocean (not shown) is also rising by about 0.5 cm over this period.

The relative contribution of the three individual terms of the right-hand-side of (5) relative to the SSH variance on timescales larger than a month is shown in Figure 16. Note the enhanced contributions of η'_{bc} along the axis of the ACC suggestive of enhanced eddy mixing and eddy heat transport across the ACC [*de Szoeke and Levine*, 1981; *Bryden*, 1979] and in the central South Pacific.

Considering the lack of model energy at the annual period, two factors need to be taken into account. The first one is related to errors in the ECMWF heat fluxes used during the model forward integration. Model heat flux errors can vary significantly in space and time and are difficult to quantify. In a recent analysis, *Siefridt* [1994] attempted to estimate ECMWF heat flux errors. Her results indicate that corrections of the order of 20 to 40 W/m^2 should be applied globally, with strong regional patterns. The ECMWF heat fluxes have even larger errors in some years, as in 1989 and 1990, when they are larger than 50 W/m^2, as a global yearly mean. (The present model simulations use 1986–1988 ECMWF monthly climatological fluxes, with the annual, global mean removed.) The relevance of those numbers for the model-data discrepancies discussed above can be easily demonstrated by a simple calculation: assuming an overall error of 25 W/m^2 and neglecting salinity effects, the steric height anomaly η'_s is related to the surface heat flux anomaly Q' by

$$\eta'_s = \frac{\alpha Q'}{\rho_0 c_p} \Delta t, \tag{9}$$

where where Q' is the assumed 25 W/m^2 surface heat flux error, $\alpha = \rho_0^{-1} \partial\rho/\partial T$ is the thermal expansion coefficient taken here to be 2×10^{-4} K^{-1}, and $c_p = 4180$ W s kg^{-1} K^{-1} is the specific heat of seawater. Applying those numbers over a period of $\Delta t = 6$ months leads to a resulting steric height uncertainty of about 1-2 cm, a number comparable to the missing amplitude in the annual cycle.

But there is nothing indicating that the heat fluxes are systematically low, suggesting that another factor appears to be relevant, residing in the missing physics of wind-induced stirring of the upper model layers which is responsible for a too small seasonal heat uptake of the model [*Sarmiento*, 1986; *Böning and Herrmann*, 1994]. As demonstrated in Figure 17a, showing the temperature history of the upper 300 m at 35°N, 30°W in the Atlantic from POCM_4B during 1989, the model tends to produce a very thin seasonal thermocline confined

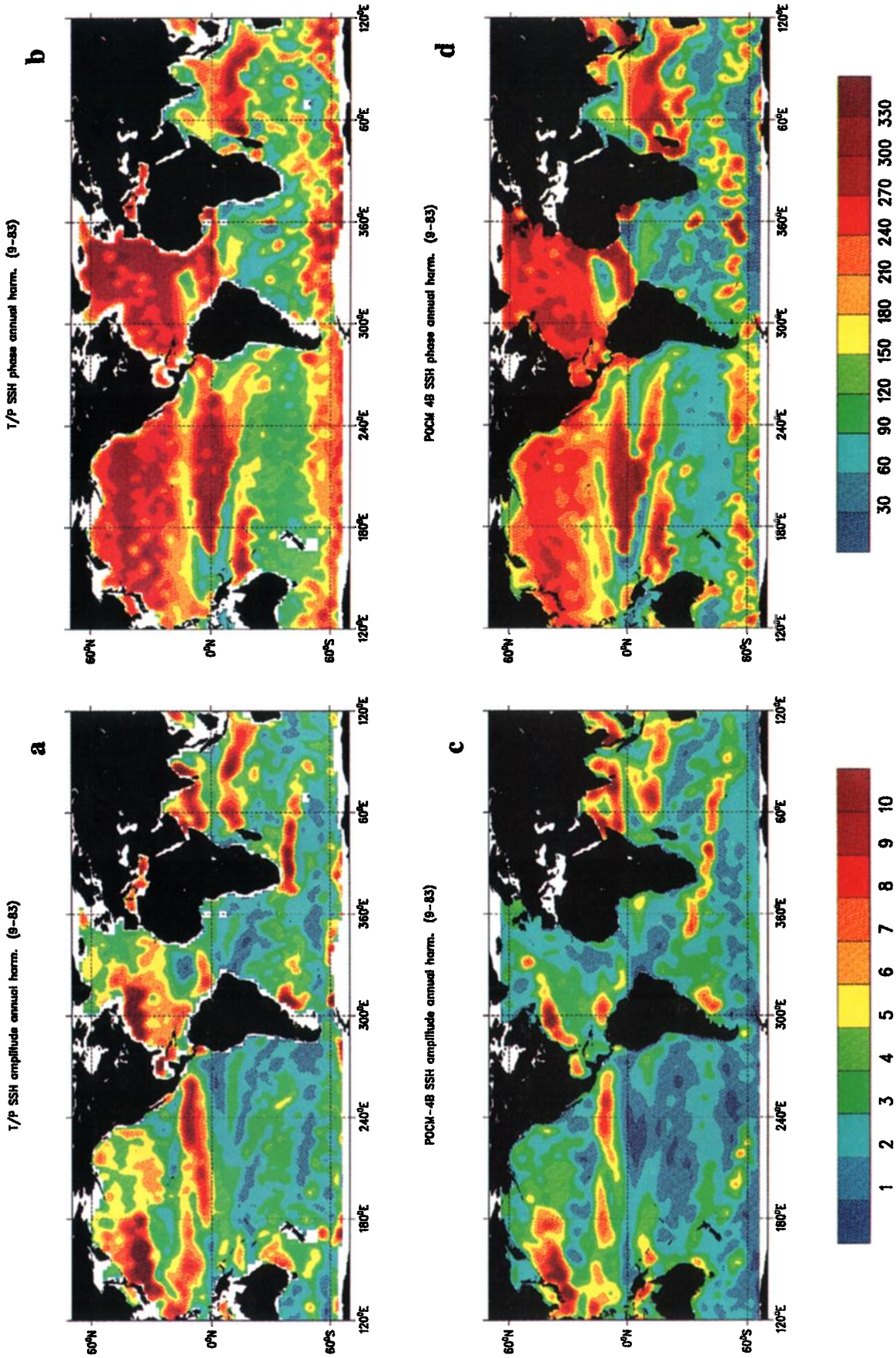

Plate 6. TOPEX/POSEIDON (a) amplitude and (b) phase of the estimated annual harmonic in sea surface height. POCM_4B (c) amplitude and (d) phase of the estimated annual harmonic in sea surface height. Contour interval is 1 cm for amplitude and 30° for phase.

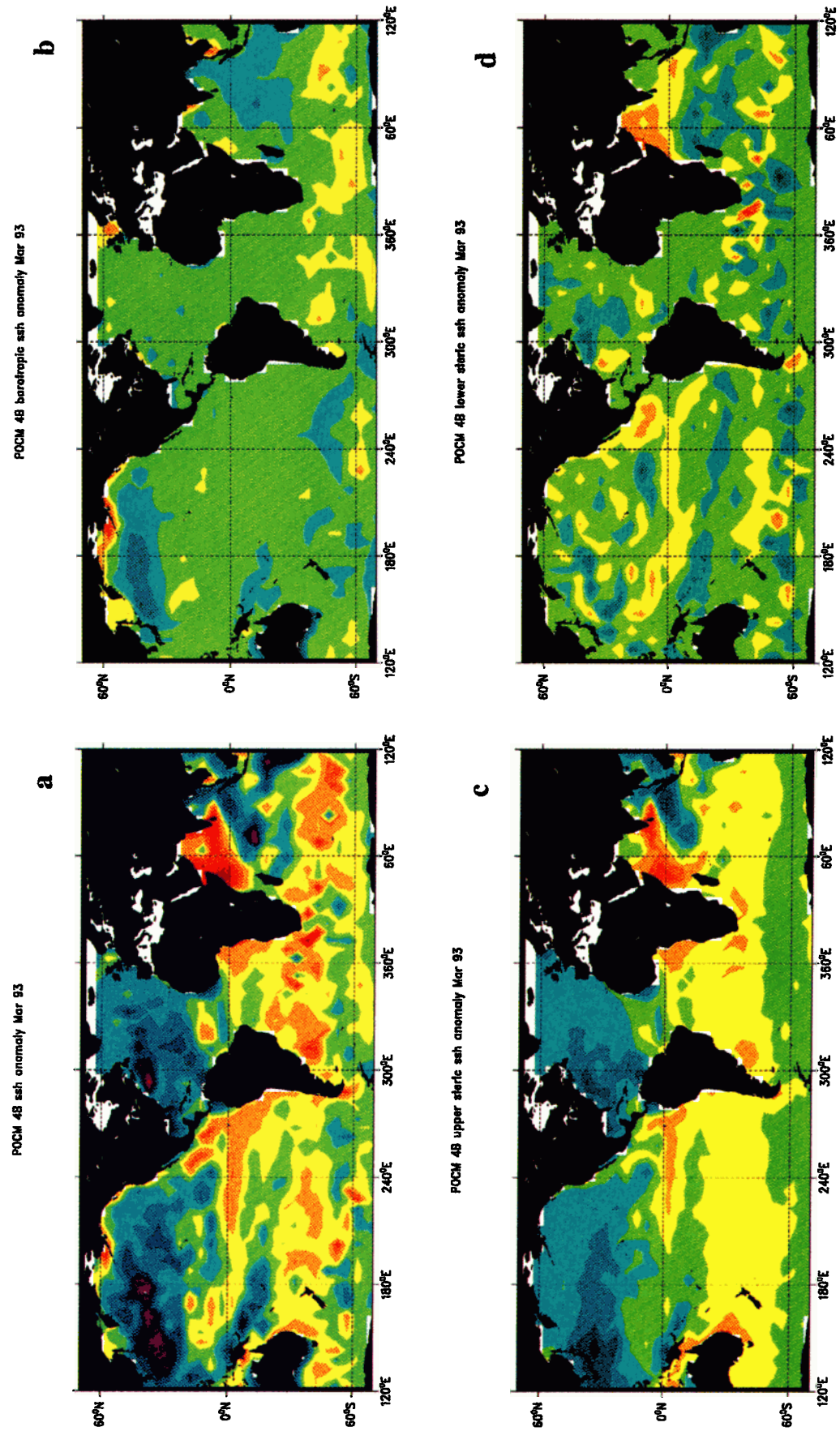

Plate 7. (a) Sea surface height anomaly relative to the 2-year mean from 1993/1994 of the monthly mean POCM_4B field in March 1993, averaged in 5° by 5° geographical areas. Also shown are the contributions of (b) the barotropic, (c) the upper layer steric and (d) the lower layer baroclinic terms to the monthly mean sea surface height field. See text for further comments. Contour interval in all fields is 1 cm.

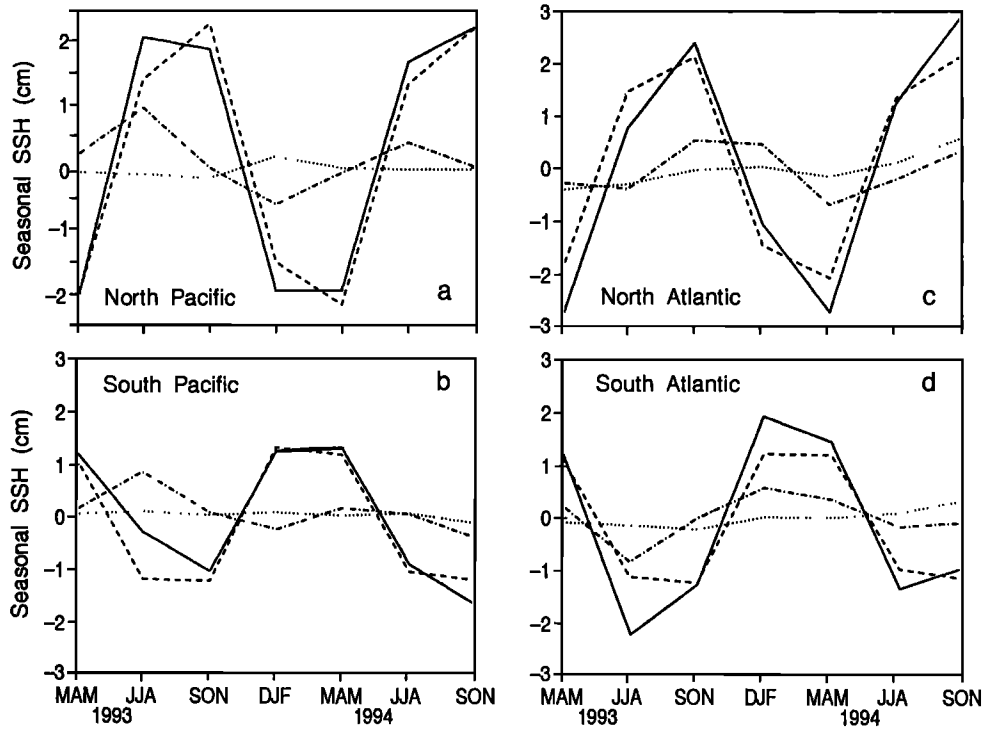

Figure 15. Decomposition of the seasonal, basin averaged model sea surface height anomalies (solid line) in terms of the contribution from the upper layer steric (dashed line), lower layer baroclinic (dotted line), and the barotropic (dashed-dotted line) component. Represented areas are again (a) 120°– 260°E, 20°– 60°N in the North Pacific, (b) 0°– 80°W, 20°– 60°N in the North Atlantic, (c) 150°– 290°E, 20°– 60°S in the South Pacific, and (d) 0°– 60°W, 20°– 60°S in the South Atlantic.

to the upper model layer with no heat uptake below. Despite the use of surface heat fluxes, its combination with a relaxation term still leads to an adjustment of the surface T fields toward Levitus climatology with the tendency away from the climatology being almost canceled by the Newtonian damping on the relaxation timescale.

However, an improvement relative to POCM_4A (Figure 17b) is still apparent (compare also with Figure 3 of *Böning and Herrmann* [1994]). Without the Barnier fluxes, literally no winter deepening of the seasonal thermocline below 75 m depth can be obtained at that location. With those fluxes, a maximum winter mixing depth of about 300 m is obtained.

The impact of a missing mixed layer physics in form of wind stirring on the vertical structure of the upper thermocline is readily apparent from the depth of the mixed layer as indicated in Figure 17a for POCM_4B. Instead of a continuous deepening of the seasonal mixing, the depth of the heated upper ocean stays constant over the summer month until convection erodes the top stratification. As a result, the heat content of the seasonal thermocline is low in the model. To quantify this statement, Figure 18 compares the vertically integrated heat content H of the upper model layers with those from *Levitus et al.* [1994] observations at the same location. Following *Gill and Turner* [1976], H is defined as

$$H = \int_{-D}^{0} [T(z) - T_{\mathrm{ref}}] dz. \tag{10}$$

$-D$ is a cutoff depth taken to be -360 m in the model and T_{ref} is evaluated as the arithmetic mean temperature at -310-m and -435-m depth.

In contrast to the seasonal march of the observed vertically integrated heat content of the thermocline where the maximum is reached in September/October and having a hysteresis (characteristic for a wind-induced mixed layer deepening with still positive surface heat budget), the model shows only half the heat storage at this particular location with variations in time along a straight line.

As demonstrated by *Böning and Herrmann* [1994], a simple parametrization of wind-induced vertical stirring of the upper model layers helps to remedy the present problem: by the related wind stirring of the top two model layers, the surface heat flux is significantly increased, reaching observed values of the zonally averaged amplitude.

6. Concluding Remarks

Led by WOCE objectives to develop models useful for predicting climate change and by the available data, our discussion has tended to focus on the differences between the model and the observations as manifested

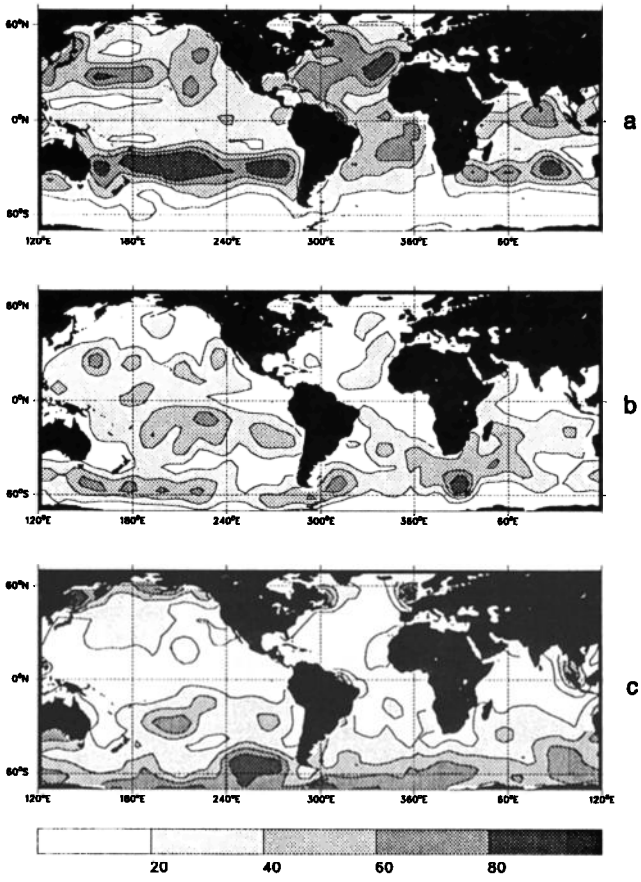

Figure 16. Percentage of variance of monthly mean SSH fields on a 5° by 5° grid due to (a) the upper layer steric component, (b) the lower layer baroclinic component, and (c) the barotropic contribution as defined in (5). Contour interval is 20%.

in the circulation in the upper thermocline, rather than model success. It therefore seems worth pausing to gain some perspective.

Most of the data we have been using were simply unavailable even 5 years ago. Furthermore, the best model solutions from even 2 years ago would have shown much greater differences from the observations than obtained here. Some of this improvement can be seen in the changes between POCM4_A and _B. There really has been progress, both on the observational and modeling fronts! We have shown here that a present state-of-the-art global OGCM simulates many aspects of the large-scale general circulation surprisingly well. Patterns of the resulting mean circulation and water mass distributions tend to reflect the observed state to the extent that the boundary conditions are known. Observed space and time structures of the large-scale variability are also successfully simulated by the model.

But there remain substantial problems. And with the increasing availability of adequate global data sets one anticipates the continuous emergence of model shortcomings. Their detailed physical understanding is the only promising strategy for further model improvements.

From this study the most prominent model failure is the general tendency toward a too weak model circulation on all scales (Figure 11). The discrepancy in SSH variability is greatest at high frequencies and wavenumbers and diminishes to about a factor of 2 at the lowest frequencies and wavenumbers accessible to us. In terms of eddy kinetic energy, K_E, we find the model simulations a factor of 4 too low as compared with T/P primarily in the mesoscale.

On long timescales, the lack of model energy, in part, is related to inappropriate surface boundary conditions. Inadequate representation of the surface mixed layer prevents the model from achieving an exchange of momentum, heat, and freshwater between the ocean and the atmosphere necessary to simulate the observed seasonal cycle in SSH and heat storage. More complete boundary layer physics is required in OGCMs.

The origin of the marked deficit in energy at all scales remains unclear: obvious candidates lie with the still too-coarse resolution or, as described above, in the use of boundary conditions which damp the smaller scales. Higher resolution appears to somewhat improve the eddy energies [*Fu and Smith*, 1996] (McClean et al., unpublished manuscript, 1996; Y. Chao, per-

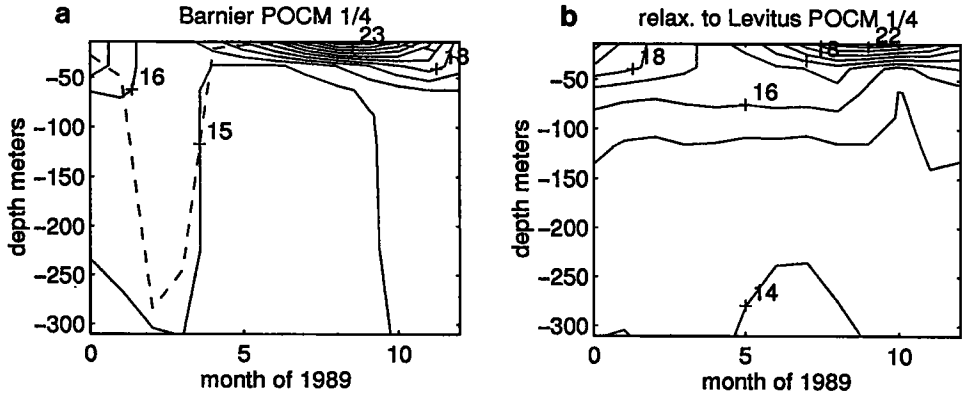

Figure 17. Temperature profile at 35°N, 35°W in central North Atlantic as a function of time during 1989 from (a) POCM_4B and (b) POCM_4A. The dashed line in Figure 17a indicates the mixed layer depth.

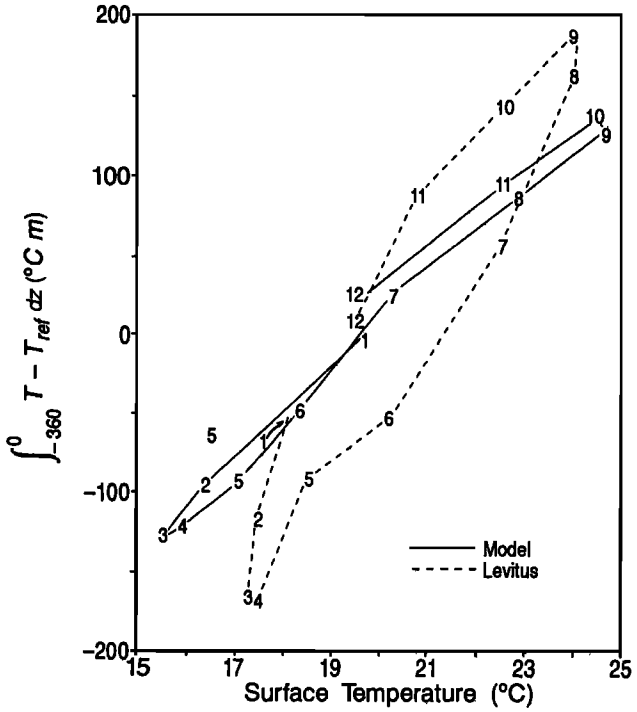

Figure 18. Heat content H at 35°N, 35°W from POCM_4B (solid line) and *Levitus* [1982] climatology (dashed line). See text for a definition of H.

sonal communication, 1996), but whether arbitrarily high-resolution will be required remains unclear. Also obscure is whether the low-frequency/low-wavenumber deficit arises from the inadequate high-frequency/high-wavenumber energy level, with the model thus failing to provide a large enough energy flux to longer scales through an upscale cascade mechanism. Uncertainties in the meteorological fields greatly complicate answering these questions as the accuracies of the long scale (time and space) forcing by the atmospheric analysis fields are unknown. For example, *Foreman et al.* [1994] have shown that two standard atmospheric analysis fields, that of ECMWF and of the U.K. Meteorological Office, produce implied southern hemisphere oceanic heat transports of opposite sign. Erroneous buoyancy forcing from the atmospheric analyses has important deleterious effects on an ocean model. Furthermore, the forcing fields used here omitted high-wavenumber/high-frequency forcing, an omission which reduces the energy levels in the forced oceanic response [see *Milliff et al.*, 1996].

Present ocean models used to simulate climate [e.g., *Delworth et al.*, 1993] are far simpler with much coarser resolution than the present one. Therefore an understanding of the consequences of the errors identified here for climate simulations is urgent. Some of the model failings represent systematic errors (e.g., the failure to move heat at high enough rates because the eddy energy is too low or because the intense boundary currents are not resolved), and such errors accumulate in model runs over decades. Understanding the causes of such errors and removing them is essential to the ultimate goal of climate forecasting.

Error characterization is equally important in any attempt to use an OGCM in combination with the observations for oceanic state estimation (or "assimilation"). Such use of a model, which is equivalent to averaging the model estimate of oceanic flows with that inferred from observations, is only rational if the relative errors of the model and the data are known and used. One is thus further driven to a focus on understanding the errors as the essential scientific element of oceanic modeling.

Acknowledgments. The authors are grateful to A. Macdonald for making her hydrographic inversion available. Brian King and Peter Saunders kindly provided the WOCE A11 data. Data from the WOCE P1, P3, P4, and A9 lines were retrieved from the public domain hydrographic data facility maintained at Scripps Institute of Oceanography. Charmaine King helped with the graphics, and C.K. Merril helped with some related early computations. Part of this work (D.S. and C.W.) is supported by contract 958125 with the Jet Propulsion Laboratory and grant NAGW-918 with the National Aeronautics and Space Administration. The Naval Postgraduate School's global modeling effort (R.T. and B.S.) is funded by the Department of Energy's Office of Health and Environmental Research under CHAMMP (Computer Hardware, Advanced Mathematics, Model Physics) and by the National Science Foundation's Physical Oceanography Program under WOCE. Computational resources for simulations were provided by the National Center for Atmospheric Research. Contribution to the World Ocean Circulation Experiment.

References

AJAX Expedition, Ajax data report, Physical, chemical and in-situ CTD data from the Ajax Expedition in the South Atlantic Ocean, aboard RV Knorr leg I, 7 October-6 November 1983, Leg II, 11 January-19 February 1984, *SIO Ref 85-24*, Scripps Inst. of Oceanogr., Univ of Calif., San Diego, La Jolla, 1985.

Barnier, B., L. Siefridt, and P. Marchesiello, Thermal forcing for a global ocean circulation model using a 3-year climatology of ECMWF analyses, *J. Mar. Syst.*, *6*, 363-380, 1995.

Beckmann, A., C.W. Böning, C. Köberle, and J. Willebrand, Effects of increased horizontal resolution in a simulation of the North Atlantic Ocean, *J. Phys. Oceanogr.*, *24*, 326-344, 1994a.

Beckmann, A., C.W. Böning, B. Brügge, and D. Stammer, On the generation and role of eddy variability in the central North Atlantic Ocean, *J. Geophys. Res.*, *99*, 20,381-20,391, 1994b.

Benada, R., Merged GDR (TOPEX/POSEIDON) users handbook, *JPL Doc. D-11007*, Version 1.0, 84 pp., Phys. Oceanogr. Distrib. Active Arch. Cent., Jet Propul. Lab., Pasadena, Calif., 1994.

Böning, C.W., and G. Budich, Eddy dynamics in a primitive equation model: Sensitivity to horizontal resolution and friction, *J. Phys. Oceanogr.*, *22*, 361-381, 1992.

Böning, C.W., and P. Herrmann, Annual cycle of polward heat transport in the ocean: Results from high-resolution modeling of the North and equatorial Atlantic, *J. Phys. Oceanogr.*, *24*, 91-107, 1994.

Brown, H.A., and K.A. Campana, An economical time differencing system for numerical weather prediction, *Mon. Weather Rev., 106*, 1025–1036, 1978.

Brügge, B., Near surface mean circulation and eddy kinetic energy in the central North Atlantic from drifter data, *J. Geophys. Res., 100*, 20,543 – 20,554, 1995.

Bryan, K., and M. Cox, An approximate equation of state for numerical models of ocean circulation, *J. Phys. Oceanogr., 2*, 510–514, 1972.

Bryden, H.L., Poleward heat flux and conversion of available potential energy in Drake Passage, *J. Mar. Res., 37*, 1-22, 1979.

Delworth, T., S. Manabe, and R.J. Stouffer, Interdecadal variations of the thermohaline circulation in a coupled ocean-atmosphere model, *J. Clim., 6*, 1993–2011, 1993.

de Szoeke, R.A., and M.D. Levine, The advective flux of heat by mean geostrophic motions in the Southern Ocean, *Deep Sea Res., Part A, 28*, 1057–1085, 1981.

Foreman, S.J., J.O.S. Alves, and N.P.J. Brooks, Assessment of surface fluxes from numerical weather prediction systems, *Tech. Rep. 104*, U.K. Meteorol. Office, Bracknell, England, 1994.

Friedrichs, M. A. M., and M. M. Hall, Deep circulation in the tropical North Atlantic, *J. Mar. Res., 51*, 697–736, 1993.

Fu, L.–L., and R.D. Smith, Global ocean circulation from satellite altimetry and high-resolution computer simulations, *Bull. Amer. Meteor. Soc.*, in press, 1996.

Fu, L.–L., and R.A. Davidson, A note on the barotropic response of sea level to time-dependent wind forcing, *J. Geophys. Res., 100*, 24,955–24,964, 1995.

Fu, L.–L., E. Christensen, M. Lefebvre, and Y. Menard, TOPEX/POSEIDON mission overview, *J. Geophys., Res., 99*, 24,369–24,382, 1994.

Fukumori, I., and C. Wunsch, Efficient representation of the North Atlantic hydrographic and chemical distribution, *Prog. Oceanogr., 27*, 111–195, 1991.

Gill, A.E., and P.P. Niiler, The theory of the seasonal variability in the ocean, *Deep Sea Res., 20*, 141–177, 1973.

Gill, A.E., and J.S. Turner, A comparison of seasonal thermocline models with observations, *Deep Sea Res., 23*, 391–401, 1976.

Greatbatch, R.J., A note on the representation of steric sea level in models that conserve volume rather than mass, *J.Geophys. Res., 99*, 12,767–12,771, 1994.

Haney, R.L., Surface thermal boundary condition for ocean climate models, *J. Phys. Oceanogr., 1*, 241-248, 1971.

Hendry, R. M., Hydrographic Measurements from C.S.S. Hudson Cruise 82-002, *Canadian Technical Report of Hydrography and Ocean Sciences, No 118*, Bedford Institute of Oceanography, Dartmouth, Nova Scotia, 112 pp., 1989.

Jacobs, S. S., and D. T. Georgi, Observations on the Southwest Indian/Antarctic Ocean, *Deep Sea Res.*, Suppl., *A Voyage of Discovery*, edited by M. Angel., pp. 43–84., Pergammon Press, New York, 1977.

Jolliffe, I.T., *Principle Component Analysis*, 271 pp., Springer Verlag, New York, 1986.

Killworth, P.D., D. Stainforth, D.J. Webb, and S.M. Paterson, The development of a free-surface Bryan-Cox-Semtner ocean model, *J. Phys. Oceanogr., 21*, 1333–1348, 1991.

King, C., D. Stammer, and C. Wunsch, The CMPO/MIT TOPEX/POSEIDON altimetric data set, *Rep. 30* 45 pp., Cent. for Global Change Sci., Mass. Inst. of Technol., Cambridge, 1994.

Klinck, J.M., Thermohaline structure of an eddy-resolving North Atlantic model: the influence of boundary conditions, *J. Phys. Oceanogr., 25*, 1174–1195, 1995.

Levitus, S., Climatological atlas of the world ocean. *NOAA Prof. Pap., 13*, 173 pp., U.S. Govt. Print. Office, Washington, D.C., 1982.

Levitus, S., R. Burgett, and T. Boyer, *World Ocean Atlas 1994*, vol. 3, *Salinity*, and vol. 4, *Temperature*, *NOAA Atlas NESDIS 3 & 4*, U.S. Dep. of Comm., Washington, D.C., 1994.

Ma, X.C., C.K. Shum, R.J. Eanes, and B.D. Tapley, Determination of ocean tides from the first year of TOPEX/POSEIDON altimeter measurements, *J. Geophys., Res., 99*, 24,809 – 24,820, 1994.

Macdonald, A., Oceanic fluxes of mass, heat, and freshwater: a global estimate and perspective, Ph.D. thesis, Mass. Inst. of Technol., Cambridge, 1995.

Macdonald, A. and C. Wunsch, A global estimate of the ocean circulation and heat fluxes, *Nature*, in press, 1996.

Mellor, G.L., and T. Ezer, Sea level variations induced by heating and cooling: An evaluation of the Boussinesq approximation in ocean models, *J. Geophys. Res., 100*, 20,565–20,577, 1995.

Mestas-Nuñez, A.M., D.B. Chelton, M.H. Freilich, and J.G. Richman, An evaluation of ECMWF-based climatological wind-stress fields, *J. Phys. Oceanogr., 24*, 1532–1549, 1994.

Milliff, R.F., W.G. Large, W.R. Holland, J.C. McWilliams, The general-circulation responses of high-resolution North Atlantic models to synthetic-scatterometer winds, *J. Phys. Oceanogr.*, in press, 1996.

Nerem, R. S., et al., Gravity model development for TOPEX/Poseidon: Joint gravity model 1 and 2, *J. Geophys. Res., 99*, 24,405 – 24,448, 1994.

Nierenberg, W, A., R. Radok, and O. M. Phillips, Physical and chemical data from the Southern Ocean between Australia and Antarctica, USNS ELTANIN Cruise 41, 1969–1970, *SIO ref. 10-72-19*, 57 pp., Scripps Inst. of Oceanogr., Univ. of Calif., San Diego, 1970.

Nowlin, W.D., Jr., T. Whitworth III, and R.D. Pillsbury, Structure and transport of the Antarctic Circumpolar Current at Drake Passage from short-term measurements, *J. Phys. Oceanogr., 7*, 788-802, 1977.

Pacanowski, R.C., and S.G.H. Philander, Parametrization of vertical mixing in numerical models of tropical oceans, *J. Phys. Oceanogr., 11*, 1443–1451, 1981.

Pattullo, J.G., Seasonal changes in the sea level, in *The Sea*, vol. 2, edited by M.N. Hill, pp. 485–496, Wiley-Interscience, New York, 1963.

Pattullo, J.G., W.H. Munk, R. Revelle, and E. Strong, The seasonal oscillation in the sea level, *J. Mar. Res., 14*, 88–155, 1955.

Peterson, R., On the transport of the Antarctic Circumpolar current through Drake Passage and its relation to wind, *J. Geophys. Res., 93*, 13,993–14,004, 1988.

Peterson, R., and L. Stramma, Upper-level circulation in the South Atlantic Ocean, *Progr. Oceanogr., 26*, 1–73, 1991.

Rahmsdorf, S., and J. Willebrand, The role of temperature feedback in stabilizing the thermocline circulation, *J. Phys. Oceanogr., 25*, 787–805, 1995.

Rapp, R.H., Y.M. Ming, and N.K. Pavlis, The Ohio State 1991 geopotential and sea surface topography harmonic coefficient model, *Rep. 410*, Dep. of Geod. Sci. and Surve., Ohio State Univ., Columbus, 1991.

Roemmich, D., and C. Wunsch, Two transatlantic sections: meridional circulation and heat flux in the subtropical North Atlantic Ocean, *Deep Sea Res., 32*, 619–664, 1985.

Roemmich, D., T. McCallister, and J. Swift, A transpacific hydrographic section along 24°N: The distribution of properties in the subtropical gyre, *Deep Sea Res., 38*, Suppl. 1A, 1–20, 1991.

Roether, W. M., Sarnthein, T.J. Müller, W. Nellen, and D. Sahrhage, Südatlantik–Zirkumpolarstrom, Reise Nr. 11, 3 Oktober 1989–11 März 1990, *Meteor-Berichte, 90–2*, Univ. Hamburg, Hamburg, Germany, 1990.

Sarmiento, J. L., On the North and tropical Atlantic heat balance, *J. Geophys. Res., 91*, 11,677 – 11,689, 1986.

Saunders, P.M. et al., RRS Discovery Cruise 199,22 Dec.1992- 01 Feb. 1993. WOCE A11 in the South Atlantic. IOSDL, *Cruise Rep. 234*, 69 pp., Wormley, Surrey, UK, 1993.

Scripps Inst. of Oceanogr., South Atlantic Ventilation Experiment (SAVE), Chemical, physical and ctd data report, legs 1, 2 and 3, *SIO ref. 92–9*, Scripps Inst. of Oceanogr., Univ. of Calif., San Diego, 1992a.

Scripps Inst. of Oceanogr., South Atlantic Ventilation Experiment (SAVE), Chemical, physical and ctd data report, legs 4 and 5, *SIO ref. 92–10*, Scripps Inst. of Oceanogr., Univ. of Calif., San Diego, 1992b.

Semtner, A.J., Jr., and R.M. Chervin, Ocean general circulation from a global eddy-resolving model, *J. Geophys. Res., 97*, 5493–5550, 1992.

Shapiro, R., Smoothing, filtering, and boundary effects, *Rev. Geophys., 8*, 358–387, 1970.

Siedler, G., and W. Zenk, WOCE Südatlantik 1991, Reise Nr. 15, Dez. 1990—März 1991, *Meteor-Berichte, 91*, pp. 126, Univ. Hamburg, Hamburg, Germany, 1992.

Siefridt, L., Validation des données de vent ERS-1 et des flux de surface du CEPMMT dans le contexte de la medélisation des circulations océaniques à l'échelle d'un bassin, Ph.D. thesis, Univ. Joseph Fourier, Grenoble, France, 1994.

Spall, M.A., Circulation in the Canary Basin: A model/data analysis, *J. Geophys. Res., 95*, 9611–9628, 1990.

Stammer, D., and C.W. Böning, Mesoscale variability in the Atlantic Ocean from GEOSAT altimetry and WOCE high resolution numerical modeling, *J. Phys. Oceanogr., 22*, 732–752, 1992.

Stammer, D. and C.W. Böning, Generation and distribution of mesoscale eddies in the North Atlantic Ocean, in *Warm Water Sphere of the North Atlantic Ocean*, edited by W. Krauss, pp. 446, Gebrüder Bornträger, Berlin, 1996.

Stammer, D., and C. Wunsch, Preliminary assessment of the accuracy and precision of TOPEX/Poseidon altimeter data with respect to the large-scale ocean circulation, *J. Geophys. Res., 99*, 24,584–24,604, 1994.

Stammer, D., and C. Wunsch, The determination of the large-scale circulation of the Pacific Ocean from satellite altimetry using model Green's functions, *J. Geophys. Res.*, in press, 1996.

Stommel, H., E.D. Stroup, J.L. Reid, and B.A. Warren, Transpacific hydrographic sections at Lats. 43°S and 28°S: The *Scorpio* Expedition, I, Preface, *Deep Sea Res., 20*, 1–7, 1973.

Talley, L.D., T.M. Joyce, and R.A. de Szoeke, Transpacific sections at 46°N and 152°W: Distribution of properties, *Deep Sea Res., 38*, Suppl., 63–82, 1991.

Tapley, B.D., et al., The JGM-3 gravity model, *Ann. Geophys., 12*, suppl. 1, C192, 1994.

Tapley, B.D., et al., The JGM-3 gravity model, *J. Geophys. Res.*, in press, 1996.

Toole, J.M., and B.A. Warren, A hydrographic section across the subtropical South Indian Ocean, *Deep Sea Res., 40*, 1973–2020, 1993.

Treguier, A.M., Kinetic energy analysis of an eddy resolving, primitive equation model of the North Atlantic, *J. Geophys. Res., 97*, 687–701, 1992.

Trenberth, K.E., J.G. Olson, and W.G. Large, A global ocean wind stress climatology based ECMWF analyses, *NCAR Tech. Note, TN-338+STR*, 93 pp., Natl. Cent. for Atmos. Res., Boulder, Colo., 1989.

Warren, B.A., Transindian hydrographic section at Lat. 18°S: Property distributions and circulation in the South Indian Ocean, *Deep Sea Res., Part A, 28*, 759–788, 1981.

Wearn, R.B., Jr., and D.J. Baker Jr., Bottom pressure measurements across the Antarctic Circumpolar Current and their relation to the wind, *Deep Sea Res., Part A, 27*, 875 – 888, 1980.

Whitworth,T., III, Monitoring the transport of the Antarctic Circumpolar Current at Drake Passage, *J. Phys. Oceanogr., 13*, 2045–2057, 1983.

Wijffels, S.E., Exchanges between hemispheres and gyres: A direct approach to the mean circulation of the Pacific, Ph.D. thesis, Woods Hole Oceanographic Inst., Woods Hole, Mass., 1993.

Woodworth, P.L., J.M. Vassie, C.W. Hughes, and M.P. Meredith, A test of the ability of TOPEX/ POSEIDON to monitor flows through the Drake Passage, *J. Geophys. Res., 101*, 11,935–11,947, 1996.

Wunsch, C., Eclectic modelling of the North Atlantic, II, Transient tracers and the ventilation of the eastern basin thermocline, *Philos. Trans. R. Soc. London, A, 325*, 201–236, 1988.

Wunsch, C., and D. Stammer, The global frequency-wavenumber spectrum of oceanic variability estimated from TOPEX/POSEIDON altimeter measurements, *J. Geophys. Res., 100*, 24,895–24,910, 1995.

Xu, W., R.J. Greatbatch, and C.A. Lin, The sensitivity of an eddy-resolving model to the surface thermal boundary condition, *J. Geophys. Res., 100*, 15,899–15,914, 1995.

You, Y., and M. Tomczak, Thermocline circulation and ventilation in the Indian Ocean derived from water mass analysis, *Deep Sea Res., 40*, 13–56, 1993.

A. Semtner and R. Tokmakian, Department of Oceanography, Naval Postgraduate School, Monterey, CA 93943 (e-mail: sbert@ucar.edu; robint@ucar.edu)

D. Stammer and C. Wunsch, Department of Earth, Atmospheric, and Planetary Sciences, Massachusetts Institute of Technology, Cambridge, MA 02139 (e-mail: cwunsch@pond.mit.edu; detlef@lagoon.mit.edu)

(Received October 17, 1995; revised April 23, 1996; accepted May 13, 1996.)